ORIGINAL PAPER

Energy landscapes and dynamics of ion translocation through membrane transporters: a meeting ground for physics, chemistry, and biology

Sunil Nath[1] ⬡

Abstract

The dynamics of ion translocation through membrane transporters is visualized from a comprehensive point of view by a Gibbs energy landscape approach. The ΔG calculations have been performed with the Kirkwood–Tanford–Warshel (KTW) electrostatic theory that properly takes into account the self-energies of the ions. The Gibbs energy landscapes for translocation of a single charge and an ion pair are calculated, compared, and contrasted as a function of the order parameter, and the characteristics of the frustrated system with bistability for the ion pair are described and quantified in considerable detail. These calculations have been compared with experimental data on the ΔG of ion pairs in proteins. It is shown that, under suitable conditions, the adverse Gibbs energy barrier can be almost completely compensated by the sum of the electrostatic energy of the charge–charge interactions and the solvation energy of the ion pair. The maxima in ΔG_{KTW} with interionic distance in the bound $H^+ - A^-$ charge pair on the enzyme is interpreted in thermodynamic and molecular mechanistic terms, and biological implications for molecular mechanisms of ATP synthesis are discussed. The timescale at which the order parameter moves between two stable states has been estimated by solving the dynamical equations of motion, and a wealth of novel insights into energy transduction during ATP synthesis by the membrane-bound $F_O F_1$-ATP synthase transporter is offered. In summary, a unifying *analytical* framework that integrates physics, chemistry, and biology has been developed for ion translocation by membrane transporters for the first time by means of a Gibbs energy landscape approach.

This article belongs to the Topical Collection: The Revolutionary Impact of Landscapes in Biology
Guest Editors: Robert Austin, Shyamsunder Erramilli, Sonya Bahar

Extended author information available on the last page of the article

Symbols

A^-	Anion
a	Hydrated ion radius (m)
d	Distance between c-rotor and a-stator in F_O portion of ATP synthase (m)
E	Local electrical field (Vm^{-1})
E	Enzyme
E	Young's modulus $(kg\ m^{-1}\ s^{-2})$
ΔG	Gibbs energy change $(kJ\ mol^{-1})$
ΔG_{sol}	Solvation Gibbs energy change $(kJ\ mol^{-1})$
$\Delta G_{desolvation}$	Desolvation Gibbs energy change $(kJ\ mol^{-1})$
H^+	Proton
$H^+ - A^-$	Proton–anion charge pair
I	Moment of inertia $(kg\ m^2)$
k	Boltzmann constant $(= 1.38 \times 10^{-23}\ J\ K^{-1})$
k	Torsional spring constant of γ-subunit in F_1 $(kg\ m^2\ s^{-2})$
$k"$	Torsional spring constant of c-subunit α-helix in F_O $(kg\ m^2\ s^{-2})$
L	Characteristic length (m)
L	Length of α-helix (m)
l	Membrane thickness (m)
l	Distance within the c-ring of F_O (m)
m	Mass (kg)
n	Number of c-subunits in the c-ring of F_O
P_n	Legendre polynomial of degree n
Δp	"Protonmotive force" $(kJ\ mol^{-1})$
q	Charge (C)
R	Inter-ionic distance within $H^+ - A^-$ charge pair (m)
R	Radius of α-helix (m)
r	Radial position (m)
r	Radial distance of a single charged species from the center (m)
T	Temperature (K)
t	Time (s)
U	Stored elastic energy $(kJ\ mol^{-1})$
z	Distance along membrane access channel (m)

Greek letters

γ	γ-Subunit of $F_O F_1$-ATP synthase
γ	$\varepsilon_W / \varepsilon_m$
ε_m	Dielectric constant of membrane
ε_w	Dielectric constant of water
ζ	Frictional coefficient $(kg\ m^2\ s^{-1})$
θ	Angle subtended by the rotating c-subunit with the center of the c-ring in F_O $(°)$
θ	Angle swept by the imaginary line joining the trailing c-rotor residue and the upper a-stator residue in F_O with respect to the equilibrium position $(°)$
θ''	Angle of rotation about the axis of the c-subunit $(°)$
λ	Inter-ionic length scale (m)
λ_D	Debye length scale (m)
ρ	Charge density $(C\ m^{-3})$

σ	Poisson's ratio
θ''	Driving electrostatic motor torque in F_O (kg m^2 s^{-2})
$\tau_{m,r}$	Resisting electrostatic motor torque in F_O (kg m^2 s^{-2})
~ 10	Net electrostatic motor torque in F_O (kg m^2 s^{-2})
Φ	Electrical potential (V)
φ	Delocalized electrical potential (V)
ψ	Local electrical potential (V)

Subscript

c	Charges in water
D	Debye
Eq	Equivalent
m	Membrane
max	Maximum
s	Solution
w	Water

Superscript

*	High-energy or transition state of intermediate

Abbreviation

Arg	Arginine
Asp	Aspartic acid
ATP	Adenosine triphosphate
Glu	Glutamic acid
His	Histidine
DASS	Divalent anion sodium symporter
K	Kirkwood
KTW	Kirkwood–Tanford–Warshel

1 Introduction

Genetic mechanisms that govern the perpetuation of living organisms and the dynamics of evolution have received considerable attention in the biological physics literature, especially from a biological perspective of "fitness" landscapes. This is primarily because biological entities, be they molecules, cell organelles, whole organisms, or ecological entities have complex interactions with their surroundings. Landscape theory is one way of describing, visualizing, characterizing, analyzing, and quantifying the dynamics of biological systems moving and evolving in space and time. The approach has been applied to evolution and natural selection [1], accelerated evolution dynamics [2], directed evolution [3], antibiotic resistance [4], and protein dynamics [5, 6].

However, the concept of energy landscapes is quite general and is not limited to being applicable only to evolutionary problems. It has been applied to diverse systems and multiscale processes in many fields, such as spin glasses, biological macromolecules, and protein folding [7–10]. It has also been generalized for arbitrary finite-range potentials using a geometrical approach [11].

The dynamic regulation of the transport of ions and polar metabolites through lipid barriers represents a vital attribute of enormous significance to living systems. Such transport is carried out by specialized enzymes and transporters embedded in biological membranes. To the best of our knowledge, a fundamental analysis that develops an *analytical framework* using Gibbs energy landscape approaches for membrane transporters in *biological* membranes has not been done, although some computational studies using all-atom molecular dynamics simulations and recent experimental studies using fluorescence resonance energy transfer on a few systems are available, often only in preprint form [12–16]. An analytical study on membrane filtration and flow through porous media treating Darcy's permeability law by the landscapes approach has recently been published [17]. However, we could not find any study that specifically treats the biomembrane-bound $F_O F_1$-ATP synthase transporter. The present article attempts to fill this gap.

The unfavorable energetics of placing a charge in a non-polar medium is a well-known effect [18–25], giving rise to an energy barrier that hinders or even prohibits charge transfer across the membrane. There exists a high desolvation Gibbs energy penalty for transferring ions from water into the membrane phase owing to this high self-energy of the charges.

Classically, the technique of voltammetry has been used to study ion-transfer reactions and transport processes at the water-organic interface and in membranes [20, 21]. Such interface reactions were found to be inconsistent with the assumption of simple, unassisted, single-step transfer processes and were proposed to involve the "formation of a *transient* ion pair at the interface" [21]. In a detailed analysis of previous works on the transport process, it was stated that, "the role of the hydrophilic ions in aqueous phases which must be distributed into the bilayer membrane together with the hydrophobic ion as the counterion to hold the electroneutrality in the membrane and aqueous phases has not been taken into account. Hence it seems difficult to understand the different features of the ion transport based on the concepts so far proposed" [20].

Several models of proton translocation through the membrane-bound F_O portion of ATP synthase have been proposed reviewed in refs. [19, 26–37]. However, none of these models has considered the large desolvation Gibbs energy penalty incurred in transferring a protonic charge from the aqueous phase into the hydrophobic membrane phase in transporters [18–25]. There exists no obvious source of energy to translocate the proton over the high desolvation Gibbs energy barrier arising from the self-energy of the charge.

It ought to be stressed that most Gibbs energy simulations in physics have focused on ion channels [38–42]. However, all membrane transporters including the $F_O F_1$-ATP synthase have very different characteristics from ion channels. Thus, transporters are alternating access, unlike channels, and translocate ions at a rate that is $\sim 10^4$ times smaller than for channels. Every known membrane transporter family is either a cotransporter or an exchanger that is engaged in coupled co-transport/exchange of at least *two* species of ions or charged metabolites, unlike channels that selectively transport a *single* ion species. Hence, the analysis made on ion channels cannot be extrapolated to transporters, which show unique properties and conformational changes.

A novel way to solve the conundrum is offered by Nath's two-ion theory of energy coupling and ATP synthesis [30–37, 43–51], formulated during a 30-year long research program on the mechanism and thermodynamics of biological molecular machines. The theory postulates the involvement of a proton and a membrane-permeable anion that approach and bind to their respective binding sites with a separation distance of ~0.5-1 nm in the access half-channels of membrane transporters and subsequently unbind to form a neutral species and exit [37, 49, 50]. This catalytic act leads to the generation of H$^+$-A$^-$ charge pair on the enzyme as the "high-energy intermediate" and results in coupling with addition and joint utilization of energy of

both ionic species, leading to rotation by ion-protein interactions [30, 34, 37, 48–50]. Nath's two-ion theory of energy coupling and Nath's torsional mechanism of energy transduction and ATP synthesis [30, 34, 37, 49, 52–55, 66] thus used the *transient*, *local* electric field arising from an ordered, sequential nature of the coupled ion transport steps for mechanical rotation, yet also satisfied the constraint of overall electroneutrality of the membrane and aqueous phases [for a review, see ref. 34, 54].

We have therefore calculated the Gibbs energy landscape/barrier for ion translocation through membrane transporters and examined to what extent the stabilizing interactions due to the coupled movement of two species of ions, e.g., anions and protons, facilitate transport and contribute to lowering of the adverse desolvation Gibbs energy barrier due to the individual ions. The ΔG calculations have been performed by using the Kirkwood–Tanford–Warshel (KTW) electrostatic theory that properly takes into account the self-energies of the ions. These calculations have been compared with experimental data on the ΔG of ion pairs in several proteins. It is shown that, under suitable conditions, the adverse $\Delta G_{\text{desolvation}}$ can be compensated by the sum of the electrostatic Gibbs energy of the charge–charge interactions and the solvation energy of the ion pair. Hence, the system is shown to become frustrated at this point via a first order phase transition involving bistability. The maxima occurring in ΔG_{KTW} as a function of the interionic distance R in the bound $H^+ - A^-$ charge pair on the enzyme is interpreted in general thermodynamic and molecular terms, and several implications for molecular mechanisms of ATP synthesis have been discussed. Finally, the timescale at which the order parameter moves between the two stable states has been estimated by solving the dynamical equations of motion, and a wealth of novel insights into energy transduction during ATP synthesis by F_OF_1-ATP synthase have been provided.

The article is organized as follows. In the Methods, Sect. 2.1 derives the leading $n = 0$ and $n = 1$ order terms of the original Kirkwood electrostatic theory that was developed for a spherical geometry. In Sect. 2.2, the Kirkwood theory is extended to the case of a membrane with planar geometry.

In the Results and Discussion, Sect. 3.1, Poisson's equation is integrated twice to obtain the local field and local potential profiles in the double lattice of a membrane containing localized positive and negative space charge regions. The profile of the Gibbs energy desolvation barrier for transport of a single charged species through a membrane is quantified in Sect. 3.2. The Gibbs energy landscape for translocation of a single charge and an ion pair is calculated as a function of the order parameter in Sects. 3.3, and 3.4 respectively, and the characteristics of the frustrated system with bistability for the ion pair are described in detail in Sect. 3.4. The theoretically calculated Gibbs energy landscape is compared with experimental data from NMR spectroscopy on a number of globular proteins in Sect. 3.5.

A general thermodynamic interpretation of analysis using continuum electrostatic Gibbs energy theories is carried out in Sect. 3.6. A molecular-level interpretation of the Gibbs energy landscape along with biological implications for ATP mechanism are spelled out in Sect. 3.7. The dynamics of movement of the system between two states is quantified by solving the equations of motion for torque production in ATP synthase, and a large number of novel insights into the energy transduction mechanism in ATP synthesis are given in Sect. 3.8. Finally, Sect. 3.9 briefly discusses how work on Gibbs energy landscapes in membrane transporters provides a meeting ground for physics, chemistry, and biology. The main conclusions of the study are summarized in Sect. 4.

2 Methods

The pioneering theory of Kirkwood [56] is employed in this work for evaluation of the Gibbs energy of charged particles. The theory was further explicated and developed by Tanford and Kirkwood [57], and modified later by Warshel [19, 38], as briefly described in Sect. 2.1. The Kirkwood theory was originally developed for a *spherical* membrane phase [56]. In Sect. 2.2, we derive an extension of the Kirkwood electrostatic theory to a *planar* membrane geometry, which provides a more accurate model of ion translocation through membrane transporters.

2.1 Kirkwood theory for calculation of electrostatic Gibbs energy

As mentioned above, in the original work [56], Kirkwood obtained the Gibbs energy of an arbitrary charge distribution placed inside a *spherical* cavity. The spherical cavity had a dielectric constant ε_m and radius L and was surrounded by an electrolyte solution of dielectric constant ε_w (Fig. 1). He solved the Laplace equation $\nabla^2\Phi = 0$ in polar coordinates (r, θ, φ) for the potential due to n charges $q_1, q_2, \ldots, q_n$ at radial positions $r, r, \ldots, r_n$ and for the reaction potential due to interaction of the charges with the surrounding solution. The work employed a combination of Dirichlet and Neumann boundary conditions which ensured that the potential and the field were continuous across the boundary of the sphere at $r = L$. The coefficients of the distance terms containing r^n in his general solution for Φ were chosen to ensure that the potential is 0 at infinity [56]. Kirkwood's final equation for the total energy of the system, including the energy of the charge–charge interactions and the interaction between the charges and the reaction potential, can be written as

$$\Delta G_K = \frac{1}{2} \sum_{k}^{n} \sum_{l \neq k}^{n} \frac{q_k q_l}{\varepsilon_m r_{kl}} + \frac{1}{2\varepsilon_m} \sum_{n=0}^{\infty} \frac{(n+1)(1-\gamma)}{(n+1)\gamma + n} \left(\frac{1}{L^{2n+1}} \right) \sum_{k}^{n} \sum_{l}^{n} q_k q_l r_k^n r_l^n P_n(\cos\theta_{kl})$$

(1)

where $\gamma = \frac{\varepsilon_w}{\varepsilon_m}$ and $P_n(\cos\theta_{kl})$ represents the Legendre polynomial.

Fig. 1 Ion pair in a membrane phase in the original Kirkwood–Tanford–Warshel (KTW) electrostatic theory [19, 38, 56, 57, 61]. The membrane has a characteristic length L and dielectric ε_m. The inter-ionic distance between the charges measures R. The dimension a represents the finite radius of the charges. The apolar phase is surrounded by a continuum aqueous phase approximated by the dielectric constant of water ε_w
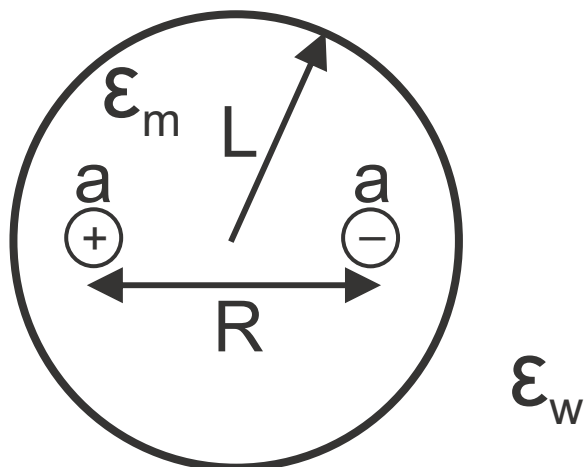
The leading $1/L$ term ($n = 0$ in Eq. (1)) gives the difference in Born energy [58] when the dielectric around a charged sphere of radius L is altered from ε_m to ε_w. The r^2/L^3 term ($n = 1$ in Kirkwood's expression) represents the energy of a dipole of length r in a sphere of radius L, where r is the distance of the charge from the center of the protein. Writing the leading $n = 0$ and $n = 1$ terms in Kirkwood's formula (Eq. (1)) for $\varepsilon_m \ll \varepsilon_w$ leads to the expression (in kJ mol^{-1})

$$\Delta G_K = -694 \left[\frac{1}{\varepsilon_m} - \frac{1}{\varepsilon_w} \right] \left(\frac{1}{L} + \frac{r^2}{L^3} \right) \tag{2}$$

Warshel later noticed that Kirkwood's expression in Eqs. (1) and (2) did not incorporate the self-energy of the charges or the finite size of the charges [19, 38]. He therefore added the electrostatic Gibbs energy of transferring a charge of radius a from the reference state (water) with $\varepsilon = \varepsilon_w$ into a membranous medium with $\varepsilon = \varepsilon_m$ to Eq. (2) so as to properly calculate the reference energy. Thus, the final equation of the Kirkwood–Tanford–Warshel (KTW) theory in kilojoules per mole for a *single* charge after including the self-energy of the charge works out to be

$$\Delta G_{KTW} = \Delta G_K + \frac{694}{a} \left(\frac{1}{\varepsilon_m} - \frac{1}{\varepsilon_w} \right) \tag{3}$$

Strictly speaking, Kirkwood's expression is not applicable for contact of charges with the surrounding aqueous solution. However, the electrostatic Gibbs energy profile is continuous, and the Gibbs energy of charges in water beyond the boundary approaches 0.

Now consider the configuration shown in Fig. 1 of a positive–negative charge pair of *two* ions of size a separated by a finite distance R embedded in a sphere of radius L of low dielectric constant, ε_m, and surrounded by a solvent of high dielectric constant, ε_w. For $\varepsilon_m \ll \varepsilon_w$, and R and L in $\overset{\circ}{A}$, we have (in kJ mol^{-1})

$$\Delta G(R)_K = -\frac{1388}{\varepsilon_m R} - 694 \left[\frac{1}{\varepsilon_m} - \frac{1}{\varepsilon_w} \right] \left(\frac{R^2}{L^3} \right) \tag{4}$$

Adding to Eq. (4) the Warshel self-energies of taking the two ions from water to the membrane protein, we obtain in kilojoules per mole

$$\Delta G(R)_{KTW} = \Delta G(R)_K + \frac{1388}{a} \left(\frac{1}{\varepsilon_m} - \frac{1}{\varepsilon_w} \right) \tag{5}$$

2.2 Extension of Kirkwood theory to a planar membrane

Figure 2 shows a double lattice containing localized regions of positive and negative charges due to an ion pair that is separated by an abrupt junction. It is shown in this section that $\Delta G(R)_{KTW}$ can also be derived analytically for the case of a planar membrane.

In order to evaluate the net ΔG modeled by $\Delta G(R)_{KTW}$, we first consider the Gibbs energy ΔG_m of two opposite charges interacting with each other and separated by a distance R inside an infinite membrane of dielectric ε_m (Fig. 2). To ΔG_m, we need to add the stabilizing Gibbs energy ΔG_w of replacing the dielectric ε_m by the dielectric ε_w at distances $r > |L|$ (Fig. 2) and subtract ΔG_c, the Gibbs energy of the charges in water at infinite separation.

Fig. 2 Extension of the KTW theory to a planar membrane. The extremities of the model lattice are taken to lie at −L and +L. Distance r is taken to be 0 at the center of the double lattice, and the electrostatic potential due to the ions is fixed as 0 at r = 0. The distance between the positive and negative charges is taken as R. The profiles of the parabolic electrostatic potential (ψ) and the linear electrical field (E) about an abrupt junction/interface at r = 0 are sketched. The exact equations for ψ and E are obtained by solving the Poisson equation directly with the appropriate boundary conditions; for the equations, please consult the text (Sect. 3.1). The physically interesting case in which electrical double layers of the positive and negative charges interact in highly localized space charge regions, e.g., for R < λ_D, or if the transporter half-aqueous access channels are characterized by the inequality 2L < λ_D, where λ_D is the Debye length is also treated in detail in the text
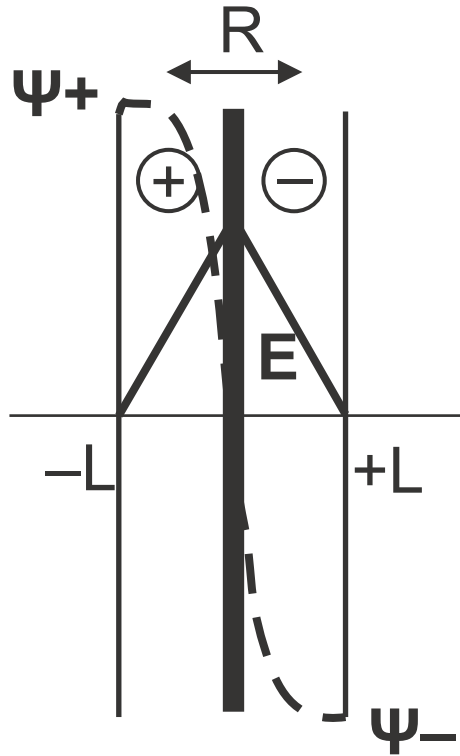
ΔG_m in kilojoules per mole works out to be

$$\Delta G_m = -\frac{694}{a}\left(1 - \frac{1}{\varepsilon_m}\right) - \frac{694}{a}\left(1 - \frac{1}{\varepsilon_m}\right) - \frac{1388}{\varepsilon_m R} \tag{6}$$

where the first term on the right-hand side is for the positive charge, the second term is for the negative charge, and the third term on the right is a measure of the charge–charge interaction. Thus,

$$\Delta G_m = -\frac{1388}{a}\left(1 - \frac{1}{\varepsilon_m}\right) - \frac{1388}{\varepsilon_m R} \tag{7}$$

Equation (7) represents the electrostatic Gibbs energy of the charges at infinite separation and the work of bringing them to approach each other to a separation distance, R.

ΔG_w is the stabilization of a dipole inside the membrane of dielectric ε_m by the aqueous solution (dielectric ε_w) with respect to its stabilization if the medium surrounding the membrane phase also possessed a dielectric ε_m. This is the Onsager energy of dipole solvation [59] shown to measure, for $\varepsilon_m \ll \varepsilon_w$ as

$$\Delta G_w = -\frac{694}{\varepsilon_m}\frac{R^2}{L^3} \tag{8}$$

Hence,

$$\Delta G = \Delta G_m + \Delta G_w - \Delta G_c = -\frac{1388}{a} + \frac{1388}{\varepsilon_m a} - \frac{1388}{\varepsilon_m R} - \frac{694}{\varepsilon_m}\frac{R^2}{L^3} - \left(-\frac{694}{a} - \frac{694}{a}\right) \tag{9}$$

i.e.,

$$\Delta G = \frac{1388}{\varepsilon_m a} - \frac{1388}{\varepsilon_m R} - \frac{694}{\varepsilon_m}\frac{R^2}{L^3} \tag{10}$$

which is the same as Eq. (5) for $\varepsilon_m \ll \varepsilon_w$. Hence, we have shown by analytical derivation that the KTW theory is applicable to both spherical and planar membrane phases.

Variation of the electrostatic Gibbs energy of the system is given by Eqs. (2) and (3) and Eqs. (4) and (5) (or by Eq. (10) for $\varepsilon_m \ll \varepsilon_w$) for a single ion or ion pair respectively as a function of R or by R/L in dimensionless terms (Figs. 1 and 2). This is important because, generally, change of Gibbs energy is reported by biochemical experimentalists as a function of R or R/L. In other words, the latter function is a kind of "order parameter" that is well known in the phase transition literature to physicists.

In Sect. 3.1, the order parameter used in chemistry and biology is related to the variation as a function of distance in the double lattice of the local field, E (Fig. 2), a variable used in physics.

3 Results and discussion

Figure 2 shows a lattice containing localized positive charge separated by a definite distance from a lattice with negative charge. Since the aspect ratio, i.e., the length/diameter ratio of membrane transporter access channels is large, and typically measures ~5–10, a one-dimensional configuration space is a good approximation and presents a useful simplification. The electrical potential and electrical field profiles can therefore be obtained by direct solution of the one-dimensional Poisson equation. In essence, our approach represents a generalization of the Shockley analysis in semiconductor physics that uses "electrons and holes" [60] to classical particles in ionic systems containing localized fixed negative and positive charges and mobile ions.

3.1 Profile of local electrical field and potential in a biological membrane containing localized space-charge regions of positive and negative charge

For both geometries shown in Figs. 1 and 2, we can write Poisson's equation as

$$\frac{d^2\psi}{dr^2} = -\frac{4\pi\rho}{\varepsilon} \tag{11}$$

On one side of the midpoint/center at $r = 0$, since the intrinsic field is the negative gradient of the local electrical potential, i.e., $E = -\frac{d\psi}{dr}$, we can write, for a single molecule with unit charge density

$$\frac{dE}{dr} = \frac{4\pi q}{\varepsilon} \tag{12}$$

which upon integration gives

$$E = \frac{4\pi q}{\varepsilon} r + C \tag{13}$$

Noting the boundary condition that

$$E = 0 \text{ at } r = -L \tag{14}$$

$$E = \frac{4\pi q}{\varepsilon} (r + L) \tag{15}$$

Similarly in the region on the other side of $r = 0$, we obtain

$$E = -\frac{4\pi q}{\varepsilon} (r - L) \tag{16}$$

Integrating again to obtain the potential, with the boundary condition that

$$\psi = 0 \text{ at } r = 0 \tag{17}$$

we finally have, on one side of the center,

$$\psi = -\frac{2\pi q}{\varepsilon} \left[(r + L)^2 - L^2 \right] \tag{18}$$

and on the other side of the center/midpoint,

$$\psi = \frac{2\pi q}{\varepsilon} \left[(r - L)^2 - L^2 \right] \tag{19}$$

The linear local field profile and the parabolic profile of the local electrical potential about $r = 0$ is sketched in Fig. 2. Hence, the order parameter given by R or by R/L can also be related to the local field, E, given its linear profile. Experimental chemists and biologists who work with NMR spectroscopy or X-ray diffraction conventionally show their results as a function of R or R/L, probably because of the difficulty of measurement of the local field within the coupling membrane, so we shall continue to follow this convention. This is all the more reasonable given the fact that we shall compare Gibbs energy landscape predictions for membrane transport with experimental data on ion pairs in various proteins subsequently (Sect. 3.5; Fig. 7).

3.2 Calculation of the desolvation Gibbs energy barrier for ion transport through membranes

The desolvation Gibbs energy (kJ mol^{-1}) arising from the self-energy of a single charge can be calculated by the Born-type formula [19, 24, 38, 61]

$$\Delta G_{\text{desolvation}} = \frac{694 q^2}{a} \left(\frac{1}{\varepsilon_{\text{m}}} - \frac{1}{\varepsilon_{\text{w}}} \right) \tag{20}$$
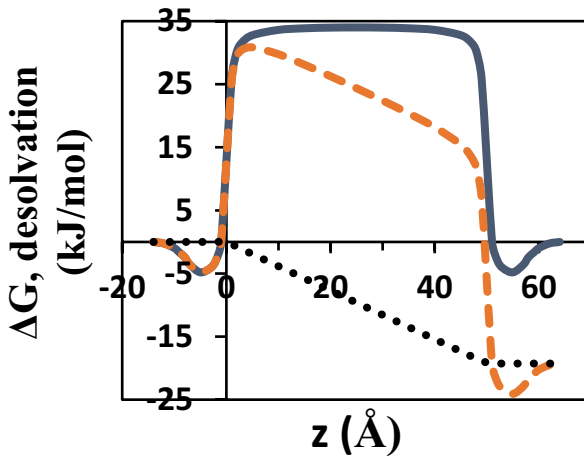
Fig. 3 Desolvation Gibbs energy barrier for *unassisted* translocation of a single ion species (e.g., H$^+$) through a biological membrane. The profile is calculated as a function of distance, z, for transfer of a unit H$^+$ charge from water into a membrane of thickness $l = 50$ Å with an effective dielectric constant $\varepsilon_m = 20$ (bold blue curve). A "protonmotive force" (Δp) of 200 mV (~20 kJ mol^{-1}) is shown by the dotted black line. The Gibbs energy barrier after superposition of the Δp is also illustrated (dashed orange curve), still revealing a substantial barrier to non-facilitated ion transport. Estimations of the effect of surface charges on the membrane at the edges $z = 0, l$ are also shown

where $q = +1$ for H$^+$, a is the hydrated radius of the ion in angstroms (on the order of 1Å), and ε_m and ε_w are the membrane and water dielectrics, respectively. For ε_m of 20, this approximately yields a maximum value of $\Delta G_{\text{desolvation energy}}$ of ~34 kJ mol^{-1} (Fig. 3). The Gibbs energy profile at an arbitrary point z within a membrane of thickness l (in Å) is given in kilojoules per mole by [61]

$$\Delta G(z)_{\text{desolvation}} = \frac{694q^2}{\varepsilon_m} \left[\frac{1}{a} - \left(\frac{1}{4z} + \frac{1}{4(l-z)} \right) \right] \tag{21}$$

which is plotted in Fig. 3 for $l = 50\,\overset{\circ}{A}$ with the constraints that ΔG tends to 0 beyond the membrane edges, i.e., at $z = -a$ and $z = l + a$. Several workers use $\varepsilon_m = 4 - 8$ and estimate considerably higher values for the desolvation Gibbs energy barrier in the range of 70–135 kJ mol^{-1} [24, 25]. Here we have taken a higher value of the dielectric in order to estimate the minimum value of the Gibbs energy barrier/landscape for *unassisted* proton translocation through biological membranes (Fig. 3). An estimate of the effect of surface charges at the membrane boundaries at $z = 0$ and $z = l$ is also shown in Fig. 3.

Current models of ion transport through membranes do not explain how this large desolvation Gibbs energy penalty is paid for by proton-translocating enzyme systems, such as the F$_O$F$_1$-ATP synthase. There exists no obvious source of energy to translocate the proton over the high desolvation Gibbs energy barrier. It should be noted that the delocalized potential, φ or the delocalized "protonmotive force" of the chemiosmotic theory, Δp of ~ 200 meV (~20 kJ mol^{-1}), is far smaller than the estimated desolvation Gibbs energy and cannot flatten the barrier (Fig. 3). Moreover, if Δp is used for reducing the height of the barrier, then no energy is available for ATP synthesis as per the chemiosmotic theory,

because the driving force for ATP synthesis, Δp, has already been consumed to reduce the desolvation Gibbs energy penalty arising from the ion self-energy.

Increasing ε_m to 15 or 20 decreases the equilibrium desolvation Gibbs energy barrier; however, it also increases the proton transfer reorganization energy, and hence, the activation barrier for proton translocation remains almost the same. Hence, the basic contradiction of the problem of too high a Gibbs energy barrier for charge transfer across the membrane is not resolved.

Nath's two-ion theory of energy coupling and ATP synthesis [30, 34, 37, 47–50] offers a way out of the above impasse. Since, according to the theory, the H$^+$ approaches the A$^-$ very closely (r ~ 0.5 – 1nm) in access half-channels in the membrane, and the H$^+$ binds within the electrostatic field of the bound A$^-$, this anionic electrical field should help lower the desolvation Gibbs energy barrier considerably. The anionic field will decrease the equilibrium value of the H$^+$ energy but will not increase the medium reorganization energy. It may even be possible to decrease the desolvation Gibbs energy penalty and barrier to 0 under special conditions.

Hence, in subsequent sections, we shall explore the electrostatic properties of ion pairs in a medium of low dielectric (membrane) surrounded by a medium of high dielectric (e.g., water).

3.3 Calculation of Gibbs energy landscapes for a single-charged species in a membrane transporter

The electrostatic Gibbs energy landscape for unassisted translocation of a single ion (e.g., H$^+$) in a membrane transporter is calculated based on Eq. (3) of the KTW continuum electrostatic theory. The dependence of the Gibbs energy as a function of distance of the charge
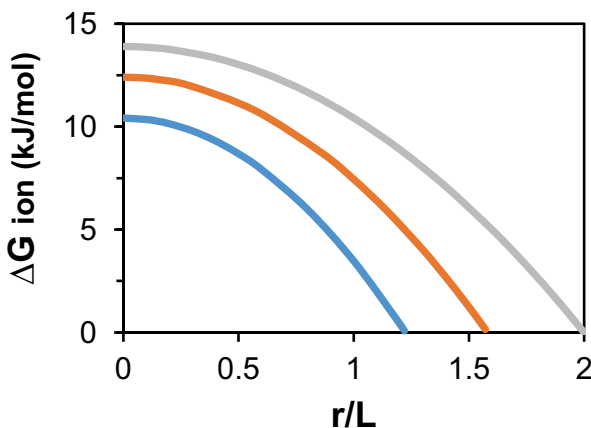
Fig. 4 Electrostatic Gibbs energy for a single type of ion/charged group of diameter a placed inside a membrane phase of characteristic length L and dielectric $\varepsilon_m = 20$ surrounded by water of dielectric ε_w $(\varepsilon_m \ll \varepsilon_w)$. Calculations of the Gibbs energy profiles are shown as a function of the order parameter r/L for various parameter values of L/a (from top to bottom) of 5.0 (gray), 3.5 (orange), and 2.5 (blue). The ΔG value is very sensitive to the position of placement of the charge. Note also that the electrostatic Gibbs energy asymptotes at $\frac{r}{L} = 0$ to the value tabulated in Table 1; therefore, the energy barrier cannot be lowered to 0 in such a charge configuration

Table 1 Expressions used and typical values of the asymptote for the electrostatic Gibbs energy change, ΔG, and the order parameter, r/L, at which the asymptotic value of ΔG is reached for a single ion ($\varepsilon_m \ll \varepsilon_w$). Similarly, the maxima in ΔG and the typical value of the order parameter, R/L, for which the maxima is obtained, are tabulated for the case of a monovalent cation–anion ion pair. Both calculations are performed based on the KTW electrostatic theory

Type of theory	Expression used for calculating the asymptotic/maximum value of ΔG (kJ mol^{-1})	Expression used for calculating the value of order parameter at which the asymptote/maximum occurs	Value of asymptotic/maximum value of ΔG for $\varepsilon_m = 20$, $a = 2$ Å, $L = 5$ Å (kJ mol^{-1})	Value of order parameter at which the asymptote/maximum occurs for $\varepsilon_m = 20$, $a = 2$ Å, $L = 5$ Å (Å)
Single ion	$\dfrac{694}{\varepsilon_m}\left(\dfrac{1}{a} - \dfrac{1}{L}\right)$	$r = 0$	10.5	0
Ion pair	$\dfrac{694}{\varepsilon_m}\left[\dfrac{2}{a} - \dfrac{3}{L}\right]$	$\dfrac{L}{\left[\varepsilon_m\left(\dfrac{1}{\varepsilon_m} - \dfrac{1}{\varepsilon_w}\right)\right]^{1/3}}$	14.0	5.5

from the center is shown in Fig. 4 for $\varepsilon_m = 20$ and various parameter values of L/a. An important feature that emerges from Fig. 4 is that the Gibbs energy asymptotes at $\frac{r}{L} = 0$ to the *destabilizing* value tabulated in Table 1; therefore, the energy barrier cannot be lowered to 0 for such a charge configuration involving only a single type of ion. Furthermore, no maxima in the Gibbs energy landscape as a function of the dimensionless distance or order parameter is found. These results are robust with respect to the choice of parameters. This arises primarily from an absence of coupling, a lack of *synergistic* action, and the inability of formation, in the absence of the anion, of the low Gibbs energy *HA* species, and the diffusion of this neutral species thereafter (i.e., after the elementary event of molecular energy transduction is completed) from the membrane phase to the outside aqueous medium. Further interpretation from the point of view of molecular mechanism is given in Sect. 3.7. The results (Fig. 4; Table 1) are quite in contrast to those obtained for an ion pair (Sect. 3.4).
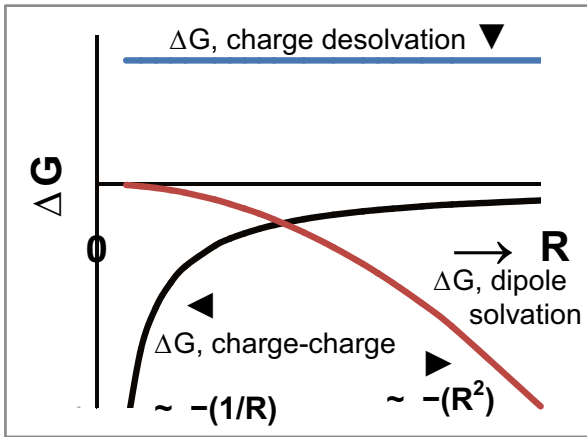
3.4 Calculation of Gibbs energy landscapes for an ion pair in a membrane transporter

In this and subsequent sections, we have attempted to determine the extent to which stabilizing interactions due to the coupled movement of *two* species of ions, e.g., anions and protons, facilitate transport, and contribute to lowering of the adverse desolvation Gibbs energy barrier due to the individual ions. The ΔG calculations have been performed by using the Kirkwood–Tanford–Warshel (KTW) electrostatic theory that properly takes into account the self-energies of the ions. These calculations have been compared with experimental data on the ΔG of ion pairs in a subsequent Section (Sect. 3.5). It is shown that, under suitable conditions, the adverse $\Delta G_{\text{desolvation}}$ can be almost completely compensated by the sum of the electrostatic Gibbs energy of the charge–charge interactions and the solvation energy of the ion pair. The maxima occurring in ΔG_{KTW} as a function of the interionic distance R in the $H^+ - A^-$ charge pair (Table 1) is interpreted in thermodynamic and molecular terms (Sects. 3.6 and 3.7, respectively) and various biological implications for molecular mechanisms of energy transduction and ATP synthesis that arise have been highlighted (Sect. 3.7). The results provide an illustration of frustrated systems with interesting bistable behavior in the physics of first-order phase transitions. The timescale at which the system moves between the two states has also been quantified for membrane transporters for the first time (Sect. 3.8).

As derived in Sect. 2 for both spherical and planar membranes (see Eqs. (5) and (10)), the basic equation of the KTW theory for the Gibbs energy of an ion pair separated by a finite distance R, which includes the Gibbs energy of taking the ions from water into the membrane, $\Delta G_{\text{KTW}}(R)$, can be recast as follows:

$$\Delta G_{\text{KTW}}(R) = -\frac{1388}{\varepsilon_m R} - 694 \frac{R^2}{L^3} \left[\frac{1}{\varepsilon_m} - \frac{1}{\varepsilon_w} \right] + \frac{1388}{a} \left[\frac{1}{\varepsilon_m} - \frac{1}{\varepsilon_w} \right] \tag{22}$$

The Gibbs energy balance associated with charge separation in membrane transporters is depicted schematically in Fig. 5. The dependence of the various components of ΔG_{KTW} (Eq. (22)) on the ion pair interionic distance, R, with respect to the reference Gibbs energy of the ions at infinite separation in water is quantified. The specific calculations shown are for $\varepsilon_m = 20$, $a = 2\,\text{Å}$, and a spherical size (or separation $2L$ in the planar geometry) of 1 nm, but the same trends are obtained for any reasonable set of parameters. $\Delta G_{\text{desolvation energy}}$

Fig. 5 Energy balance associated with Gibbs energy landscapes for ion pair translocation through membrane transporters. The variation of the components of ΔG on the ion pair interionic distance, R, is plotted. The large destabilizing desolvation Gibbs energy penalty due to the self-energy of the charges is shown (blue). The stabilizing Gibbs energy of the charge–charge interaction scales as $-(1/R)$ (black), while the stabilizing Onsager energy for dipole solvation (red) follows a $-(R^2)$ relationship. Calculations are based on Eq. (22) for $\varepsilon_m = 20$, $a = 2\,A$ and a protein characteristic size of 1 nm. Similar trends are obtained for other sets of parameter values. The reference Gibbs energy of the ions at infinite separation in water is taken as 0

due to the self-energy of the charges shows up as a large positive destabilizing value that is independent of R. On the other hand, $\Delta G_{charge-charge}$ is negative (stabilizing), scales as $-(1/R)$, and goes from a negative infinity value as the bonding distance tends to 0, as would occur, for example, in the neutral substrate HA, to a value close to 0 for long-range ion pairs (Fig. 5). $\Delta G_{\text{dipole solvation}}$, the stabilizing Onsager energy, follows a parabolic $-(R^2)$ relationship that goes from 0 at a bonding distance between the ion pair to a large negative value for long-range ion pairs (Fig. 5). From the various contributions shown in Fig. 5, it can be readily inferred that an apparently small value of $\Delta G_{KTW}(R)$ can result at small $(R < 4\text{Å})$, for a neutral substrate HA, and for long-range ion pairs $(R \sim 8 - 10\,A)$ due to compensation of the destabilizing self-energy term and the sum of stabilizing Gibbs energy contributions of $\Delta G_{KTW}(R)$ (Fig. 5). Furthermore, a maxima in $\Delta G_{KTW}(R)$ is expected to be found at an intermediate value of the interionic distance, R, corresponding to a $H^+ - A^-$ "high-energy charge-pair intermediate".

Figure 6 calculates the Gibbs energy of an ion pair with inter-ionic separation R placed inside a membrane phase ($\varepsilon_m = 20$) surrounded by water of dielectric $\varepsilon_w (\varepsilon_m \ll \varepsilon_w)$. Calculations of the Gibbs energy landscapes are shown as a function of the order parameter R/L for various parameter values of L/a. Recombination of the two charges of the ion pair ($R \to 0$) *after* ion unbinding from their respective binding sites in the membrane transporter leads to a lowering of the Gibbs energy barrier to 0 in such a paired charge configuration.

The electrostatic Gibbs energy involving an ion pair (Fig. 6) can be regarded as an interesting example in physics of a *frustrated* system with *bistability* that shows a *maxima* at intermediate values of R/L. The system reveals two values of the order parameter, R/L, with the same minimum value of Gibbs energy (Fig. 6). Thus, the net ΔG_{KTW} tends to a value of ~ 0 at a finite separation distance of H^+ and A^- owing to almost complete Gibbs energy compensation. A second stable state with a minimum in total Gibbs energy
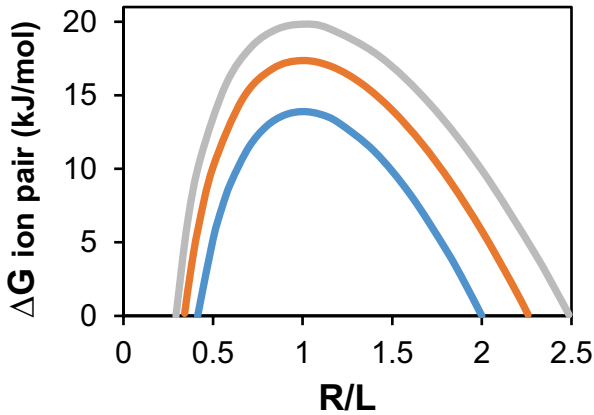
Fig. 6 Electrostatic Gibbs energy of an ion pair with inter-ionic separation R placed inside a membrane phase ($\varepsilon_m = 20$) surrounded by water of dielectric ε_w ($\varepsilon_m \ll \varepsilon_w$). Calculations of the Gibbs energy landscapes are shown as a function of the order parameter R/L for various parameter values of L/a (from top to bottom) of 3.5 (gray), 3.0 (orange), and 2.5 (blue). Note that the electrostatic Gibbs energy shows a maxima at intermediate values of R/L, as tabulated in Table 1. Recombination of the two charges of the ion pair ($R \to 0$) *after* ion unbinding from their respective binding sites in the membrane transporter leads to a lowering of the Gibbs energy barrier to 0 in such a paired charge configuration. In this mode of ion translocation, the two ions move in a coupled way and bind specifically in correlated states at a finite distance of separation, R, before their unbinding from their sites occurs

is obtained for formation of a chemical bond (i.e., for $R \to 0$) to yield the charge neutral substrate HA. In between these two stable states, there exists a barrier in the Gibbs energy landscapes (Fig. 6) with a high Gibbs energy state of $H^- - A^-$ at a definite distance of separation. The maxima in ΔG_{KTW} for the ion pair system occurs at

$$R_{max} = \frac{L}{\left(\varepsilon_m \left[\frac{1}{\varepsilon_m} - \frac{1}{\varepsilon_w} \right] \right)^{\frac{1}{3}}} \tag{23}$$

or, for $\varepsilon_m \ll \varepsilon_w$ at $R_{max} \approx L$. For $\varepsilon_m \ll \varepsilon_w$, this yields the maximum Gibbs energy change (in kJ mol^{-1})

$$\Delta G_{KTW, max} = \frac{694}{\varepsilon_m} \left[\frac{2}{a} - \frac{3}{L} \right] \tag{24}$$

These values are tabulated in Table 1. The difference between the maximum value of the Gibbs energy barrier and the ground state Gibbs energy (Table 1; Figs. 6 and 7) is available to perform useful mechanical work in a membrane transporter such as the F_OF_1-ATP synthase. This works out over a 120° catalytic cycle of ATP synthesis to a stored energy in a *nonequilibrium* state of an enzyme subunit — or in a local region/mechanical degree of freedom of the system — corresponding to ~60 kJ mol^{-1}, a quantum of energy that is sufficient to synthesize one mole of ATP [47, 50, 54, 62].

The results shown in Fig. 6 constitute a classic example of a first-order phase transition in physics with a free energy barrier separating two values of the order parameter with the same minimum value of Gibbs energy. The *timescale* at which the order parameter moves abruptly between the two values has proved difficult to define for many physical systems.
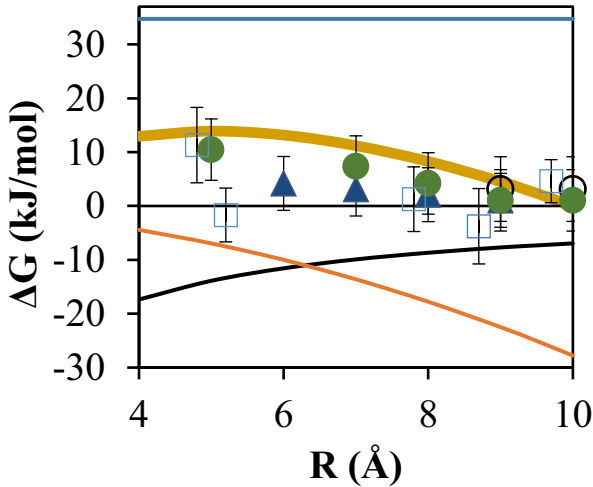
Fig. 7 Comparison with experimental data of the calculated Gibbs energy landscapes for ion pairs upon their transfer from water into the membrane transporter. The ΔG of the various components and the total ΔG are calculated by the KTW electrostatic theory. The sum of the desolvation Gibbs energy of the two species of ions (horizontal blue line), the Gibbs energy change of charge-charge interactions between positive and negative ions (black curve), the Gibbs energy change of dipole solvation (orange curve), and the *net* ΔG change (thick ocher curve) are plotted. Calculations are shown as a function of R for $\varepsilon_{\mathrm{m}} = 20$ and $a = 2\text{Å}$ for a 1-nm diameter of an individual c-subunit constituting the c-oligomer in the membrane-bound F_O portion of a single molecule of the $F_O F_1$-ATP synthase. The reference Gibbs energy of the ions far apart in water is taken as the boundary condition, which asymptotes to 0 beyond the right edge of the figure. Experimental measurements of the total Gibbs energy change for interactions in proteins and in water are plotted, and mean and *SD* values are shown. Estimates are based on NMR ensemble data for long-range ion pairs (open square) [77]; heme groups and surface charges in cytochrome c (open circle) [78]; ion pairs in hemoglobin, lysozyme, and cytochrome c (filled circle) [79–81]; and dicarboxylic acids in water (filled triangle) [38]

However, for membrane transporters, the timescale at which the order parameter transitions in a *discrete* step between the two stable states has been calculated for the first time by solving the dynamical equations of the system (see Sect. 3.8).

3.5 Comparison of theoretically predicted landscape with experimental data on proteins

A major goal of this work is to calculate of the Gibbs energy landscape upon moving an ion pair from water to the low dielectric medium of a membrane transporter and compare them with experimental ensemble NMR data. The ΔG of the various contributions for such a transfer and the total ΔG have been calculated from KTW theory based on Eq. (22) and plotted in Fig. 7. The effective radius of H_3O^+ is estimated using the Born formula [58] for $\varepsilon_{\mathrm{m}} \ll \varepsilon_{\mathrm{w}}$ as $a = -694/\Delta G_{\mathrm{sol}}$, where ΔG_{sol} is the solvation Gibbs energy of H_3O^+ in water, which is taken as -418 kJ mol^{-1}. Calculations are shown as a function of R for $\varepsilon_{\mathrm{m}} = 20$, $a = 2 A$, and 1 nm effective size of an individual c-subunit [28, 30] that constitutes the c-ring in the membrane-bound F_O portion of ATP synthase (Fig. 7). The reference Gibbs energy of the ions far apart in water is taken as 0. Experimental estimates of the total Gibbs energy change for interactions in various proteins and water are shown, and mean and *SD*

are also given. The calculated values can thereby be readily compared with experimental data on ion pairs, and reasonably good agreement between theory and experiment is obtained (Fig. 7).

3.6 Thermodynamic interpretation of continuum electrostatic Gibbs energy theories

A thermodynamic interpretation can also be provided for the Gibbs energy calculations in Sects. 3.4 and 3.5 and the results shown in Figs. 5–7. It can also help elucidate if pairing of ions of opposite charge can assist ion permeation and translocation in membrane transporters. Let the two ions be labeled H^+ and A^- and let the aqueous and apolar membrane phases be given the symbols w and m, respectively.

We define $\Delta G_{H^+, w \to m}$ and $\Delta G_{A^-, w \to m}$ as the Gibbs energies of transfer of the individual protons and anions from water into the membrane phase. Furthermore, $\left(\Delta G_{H^+A^-, m} - \Delta G_{H^+A^-, w}\right) = \Delta\Delta G_{H^+A^-, w \to m}$ is defined as the change in interaction/binding Gibbs energy upon transfer of the ion pair from aqueous medium, w, into the membrane phase, m. With these definitions, the Gibbs energy change for transfer of the *ion pair* from phase w to phase m, $\Delta G_{H^+A^-, w \to m}$ is given by the general thermodynamic equation

$$\Delta G_{H^+A^-, w \to m} = \left(\Delta G_{H^+A^-, m} - \Delta G_{H^+A^-, w}\right) + \Delta G_{H^+, w \to m} + \Delta G_{A^-, w \to m} \qquad (25)$$

Equation (25) enables interpretation of various continuum electrostatics Gibbs energy transfer theories in terms of chemical thermodynamics. Thus, $\Delta G(R)_K$ in Eq. (4) of Sect. 2.1 that contains the leading $n = 0$ and $n = 1$ order terms of Kirkwood's theory (Eq. (1); Sect. 2.1) can now be interpreted as an estimate of the stabilizing change in interaction Gibbs energy, $\Delta\Delta G_{H^+A^-, w \to m}$ upon transfer of the ion pair from a polar phase, w, into an apolar membrane phase, m. These favorable interactions are interpreted electrostatically by the Kirkwood theory as a sum of charge–charge and Onsager dipole solvation energies and are quantified in Figs. 5–7. The destabilizing $\Delta G_{H^+, w \to m} + \Delta G_{A^-, w \to m}$ terms in Eq. (25) are satisfactorily taken into account by Warshel's important extension of Kirkwood-Tanford theory in order to consider the finite size of the charges along with the appropriate inclusion of the charge self-energies. These destabilizing components are given by the second term on the RHS of Eq. (5) or the first term on the RHS of Eq. (10) within KTW theory.

The above has several thermodynamic consequences. For example, transfer of a *single* ion such as H^+ from phase *w* to phase *m* entails a desolvation Gibbs energy penalty $\Delta G_{H^+, w \to m}$ that is quantified in KTW theory by the charge self-energy $\frac{694}{a}\left[\frac{1}{\varepsilon_m} - \frac{1}{\varepsilon_w}\right]$ (kJ mol^{-1}). Models of energy coupling, such as the chemiosmotic theory, that fail to include key self-energy terms and ignore fundamental charge desolvation effects cannot provide an adequate description of ion translocation through the F_OF_1-ATP synthase and other membrane transporters.

Finally, other semi-macroscopic or microscopic electrostatic theories can also be interpreted within the general thermodynamic framework given by Eq. (25), as shown here for the KTW theory. Thus, with progress, electrostatic Gibbs energy theories can be embellished and further sophisticated to help provide ever-increasing and more detailed insights into the contributions and effects of the various stabilizing and destabilizing interactions in enzymes, transporters, and other biological molecular machines.

3.7 Molecular interpretation and biological implications

Figure 7 illustrates that the net ΔG_{KTW} tends to a value of ~ 0 at a finite separation distance of H^+ and A^- (~10Å under the conditions in Fig. 7) owing to complete Gibbs energy compensation due to ion-ion coupling by local fields. In principle, this localized coupling *within* membrane transporters arises physically due to interaction between the diffuse electrical layers around the positive and negative space-charge regions (Sect. 3.1). More rigorously, if λ is the inter-ionic distance between the bound positive and negative charges, and λ_D is the Debye length in the aqueous electrolyte of the half-access channels of the membrane transporter, we should have, for coupling

$$\lambda \sim R \approx L < \lambda_D \tag{26}$$

For a univalent 10-mM electrolyte at 25 °C, the Debye length, λ_D measures 3 nm. Hence, as seen, for example, from Fig. 7, the inequality given by Eq. (26) is satisfied for access channels *within* membrane transporters. Thus, an analysis of system scale sizes helps shed light on molecular mechanism [63].

On the other hand, in the electrolyte solution/interface with the overall membrane, e.g., periplasm/cytoplasm, or matrix/inner membrane in mitochondria, an analysis of scaling in the mesoscopic system [63] shows that $\lambda > \lambda_D$. Hence, for the membrane *as a whole*, the electrical field in the surrounding aqueous phases does not persist beyond length scale λ_D, and hence, there can be no overlap of electrical layers of the charges in the solution. Thus, these aqueous spaces are electrically *quasi-neutral*.

The principle can be formulated that in order to create conditions for overlap of electrical layers (and thereby local coupling), i.e., $\lambda < \lambda_D$, a localized confined region or space *within* the membrane is necessary, as for example, around an access channel. This differs from the conventional capacitance involving the entire membrane leaflet separating two electrolyte solutions on either side of it, generally shown as charged. The charges are considered to be located either in the bulk aqueous media (as in chemiosmosis) [27, 64] or at the membrane surface [26, 65].

Moreover, as explained in detail in Sect. 3.4, a second stable state with a minimum in total Gibbs energy is obtained for formation of a chemical bond (i.e., for $R \rightarrow 0$) to yield the charge neutral substrate *HA*. In between these two stable states, there exists a high Gibbs energy state of $H^+ - A^-$ on the enzyme, i.e.,$[E-H^+A^-]^*$, at a definite distance of separation, R (see Eqs. (23) and (24); Table 1; Figs. 6 and 7).

Thus, at the molecular level, oppositely charged ions translocate from a bulk aqueous phase along their concentration gradients sequentially and in a coupled way and bind to their respective binding sites in the membrane of a single enzyme/transporter (i.e., cotransporter or exchanger) molecule, and local fields are created in the membrane transporter around the ion-binding sites. *Charge separation of the ion pair thus occurs and the bound $H^+ - A^-$ charge pair on the enzyme/transporter can be regarded as an "high energy intermediate." This high-energy state of the enzyme is subsequently discharged and utilized for the performance of useful work by ion-protein interactions.* During this energy transduction process, the Gibbs energy maximum is lowered by the interaction of the bound charges with the protein in the membrane (ion-protein interactions), e.g., at the sharp a–c interface/junction in the membrane-bound F_O portion of ATP synthase [30, 34, 49, 53]. This interaction has conformational characteristics and leads to rotation in the membrane-bound F_O portion of ATP synthase by means of a mechanoelectrochemical process that is transmitted to the extra-membrane F_1-portion of ATP synthase, as explained in detail by Nath's

torsional mechanism of energy transduction and ATP synthesis [30, 34, 49, 52–55, 66, 67]. After unbinding from their respective binding sites in the membrane, the H^+ and A^- recombine to form neutral substrate *HA*, which is the second state of low ΔG_{KTW}, and thereafter the HA molecule leaves the enzyme. In summary, the separation and recombination of ion pairs constitute the elementary events in biological energy transduction and storage in membrane transporters.

The above has major implications for molecular mechanisms of biological energy transduction and points to a central role for *interactions* between the ions and the enzyme/transporter system. The bound ions help to generate "an energized state" of the enzyme/transporter in *local* membrane domains. The enzyme/transporter facilitates the separation of the positive and negative charges of an ion pair to definite distances by lowering the Gibbs energy required for this process and enables thereafter their recombination to form the uncharged substrate molecule. Since this is a reversible process, the enzyme can also catalyze the reverse hydrolysis reaction in other biological processes and act as an hydrolase, e.g., as F_1-ATPase.

As desired by one of the reviewers, the above molecular explanation offered for enzyme-catalyzed reactions is compared to that for an ordinary chemical reaction. In the conventional view of catalysis, the reaction progresses from a set of chemical bonds in the reactants to another, different sets of bonds in the products, and the role of the catalyst is to lower the activation Gibbs energy of the reaction. The activated state may contain separated charges; however, their concentrations are considered to be negligible. In our mechanism, the enzyme not only alters reaction rates but it also alters the type of product. For example, the mechanism shows that chemical bonds need not be broken to be replaced by a different set of bonds, but can also be replaced by stable charge-separated species (or vice versa).

The above discussion has clarified that in biological energy transduction, the ability of a membrane-bound enzyme/transporter to remove a positive and a negative charge from a neutral substrate, stabilize them, for example, by binding to specific binding sites, and thereby, separate charges at definite distances are of paramount importance in bioenergetics. The separated charges can interact with each other and with the protein, causing conformational changes within the designed protein structure and medium *without dissipation of energy*. These possibilities of a network of interactions of the *separated* charged pairs are not generally available for ordinary chemical reactions.

The above concepts are illustrated by means of a Gibbs energy vs. progress of reaction diagram in Fig. 8. Shown therein is the Gibbs energy as a function of the separation of a positive and negative charge. The minimum in Gibbs energy at r=0 in the medium corresponds to a chemical bond, while the minimum at a separation r_s corresponds to separated charges. Ideally, the Gibbs energy minimum of these two stable states should be equal (Fig. 8). If the separated charges occur in aqueous solution on one side of the membrane, then we can assign a reference value of 0 to the Gibbs energy, as shown by the bold curve. If the neutral undissociated species HA at r=0 in the medium of the transporter diffuses outward and exits to an aqueous medium on the other side of the membrane, it will exist as H^+A^- in the aqueous phase on the other side of the membrane and still possess the reference value of 0 Gibbs energy. If, on the right-hand side of the diagram, the charges could be separated further, beyond r_s, then the electrostatic Gibbs energy of the system will increase further (dashed curve in Fig. 8). However, there is no logical reason, once the enzyme medium recognizes two separated charges, why it will facilitate further charge separation because the Coulombic attraction between the two charges will resist larger separation. *The creation of a transient, finite-time, high-energy charged pair intermediate on*
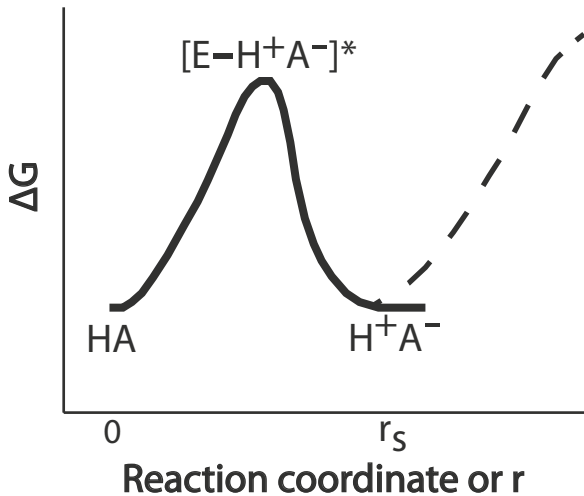
Fig. 8 Gibbs energy as a function of reaction progress/distance of separation of a positive and negative charge for an enzyme-catalyzed reaction. r = 0 corresponds to a chemical bond, while the minimum at a separation r_s corresponds to separated charges in solution. The essential high-energy charged pair intermediate on the enzyme is represented by $[E-H^+A^-]^*$. The difference between the value of the electrostatic Gibbs energy of $[E-H^+A^-]^*$ at the maximum of the barrier and the reference energy at the minima (bold curve) is transduced to useful mechanical work by the system. If the charges are separated beyond distance r_s, then the electrostatic Gibbs energy of the system increases further (dashed curve). However, Coulomb attraction between the two charges will resist separation $>r_s$

the enzyme, $[E-H^+A^-]^*$, *and its destruction is key to the elusive process of energy transduction.* The difference between the value of the electrostatic Gibbs energy of $[E-H^+A^-]^*$ at the maximum of the barrier and the reference Gibbs energy at the minima (Fig. 8) is transduced to useful mechanical work by the system.

It should be stressed that the above model of biological energy transduction is quite different from the usual model in which the membrane is essentially considered a solid dielectric of packed lipids with a dielectric constant of ~5 that separates electrically conducting media/water on either side across which ion translocation occurs. Looking at our space charge model in a macroscopic way, energy storage is due not to the dielectric between two aqueous media/conductors but to a gradient of immobile charges of opposite sign within a dielectric matrix in which mobile ions are distributed throughout in accordance with the Poisson equation. In the double lattice, the junction of bound positive and bound negative charges gives rise to a transition region which is depleted of mobile ions and therefore possesses high space charge density, almost equal to the fixed charge concentration. In contrast, regions that are distant from the lattice junction have a small space charge density.

As explained above, bound charges uncompensated by mobile counterions lead to strong space charge regions. The electrical field in the depletion layer, which has a thickness of 1-2 nm under physiological conditions, is very high. For a fixed charge concentration of 100 mM, and a dielectric constant between 10 to 20, the (transient) local field for an abrupt fixed charge density profile would be on the order of 10^6 V cm^{-1}, even when no electrical potential is imposed across the membrane. Thus, in the presence of steep transition regions of bound charges of opposite sign, as in the double lattice (Sect. 3.1) when two lattices of opposite sign are *juxtaposed*, the system displays conservative properties, and

electrostatic energy storage can readily occur by perturbation of the space charge. In the absence of such localized space charge layers, homogeneous aqueous electrolyte solutions would be primarily resistive in nature.

Finally, it ought to be emphasized that Mitchell's chemiosmotic theory, being a bulk phase to bulk phase theory according to which only external aqueous media are assumed to be energized, and only the delocalized electrical potentials φ arising from such energization are considered [27, 64], cannot offer any meaningful insights into such *local* molecular coupling processes occurring within membrane transporters. On the other hand, Nath's torsional mechanism of energy transduction and ATP synthesis and Nath's two-ion theory of energy coupling considers events occurring inside the energy-transducing membrane and can therefore greatly contribute to understand and quantitatively model realistic *intramembrane* molecular energy transduction processes (Sect. 3.8).

3.8 Calculation of the timescale of movement between two stable states and quantification of the rotary dynamics of $F_O F_1$-ATP synthase

The timescale at which the enzyme/transporter moves between two stable states of a frustrated system can be estimated by simulation of the dynamics of torque generation in the $F_O F_1$-ATP synthase as a model example. In Nath's two-ion theory of energy coupling, a dynamically electrogenic but overall electroneutral ion transport involving membrane permeable anions (such as succinate) and protons has been postulated. In order to utilize the energy of the anion gradient, the anion flows along its concentration gradient to its conserved binding site on the a-subunit of the membrane-bound F_O portion and creates a local $\Delta\psi$. This local potential is the signal for proton translocation along its concentration gradient, and the proton binds to its conserved binding site on the c-subunit of F_O. Thus, torque generation is a result of change in electrostatic potential, $\Delta(\Delta\psi)$ brought about by the binding of proton moving along its concentration gradient to its binding site on the c-subunit that lies within the electrostatic potential field of the bound anion on the a-subunit stator at the abrupt a–c interface/junction within F_O.

A charge geometry at the a–c interface containing bound ion pair and consensus conserved residues for modeling torque generation in the F_O portion of ATP synthase [30] is shown in Fig. 9. The model uses two mutually non-colinear half-access channels, whose existence had been predicted by us ([28, 53]; for a review, see especially pp. 88–93 and Fig. 12 of [30]), several years before structural studies on the ATP synthase by X-ray and cryo-EM techniques revealed their presence [68–70]. Thus, entry and exit of protons through the corresponding half-channels are separated by the time it takes the c-rotor to rotate by 15° (for twelve c-subunits in the c-ring). It should be noted that the torsional mechanism works equally effectively for other values of the number of c-subunits constituting the c-oligomer, as shown earlier [54].

In the charge geometry of Fig. 9, l_{23} is the distance between the two negatively charged c-rotor residues and d the channel distance between the rotor and the stator, or more precisely, the distance in space separating the residues harboring the positive and negative charges, which can be smaller than the channel thickness. We represent the vertical offset between the leading negatively charged rotor residue and the upper positively charged a-stator residue by r_{12}. The vertical offset between the trailing negatively charged rotor residue and the lower positively charged stator residue is represented by r_{34}, while the horizontal offset is denoted by l_{34}. θ is the angle subtended by the rotating c-subunit at any instant of time with the center of the c-ring. θ' is the angle swept by the imaginary line joining the
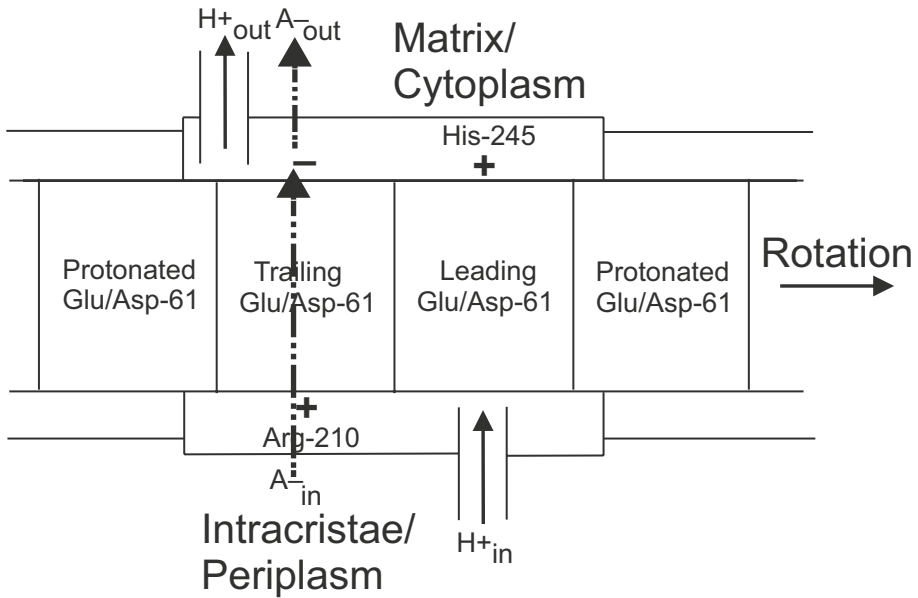
Fig. 9 Charge geometry for torque generation and unidirectional rotation of the c-ring with respect to the a-subunit stator in the membrane-bound F_O portion of the F_OF_1-ATP synthase transporter. The conserved Arg-210 and His-245 amino acid residues (*Escherichia coli* numbering) on the a-stator are depicted by the + symbols. Dicarboxylic acid anion, e.g., succinate (dashed line), translocates along its concentration gradient and binds to its conserved a-subunit site [47, 49–51, 62, 63, 82], indicated by the minus symbol, creating a local $\Delta\psi$. H^+ ion (bold line) subsequently translocates along its concentration gradient through the two mutually non-colinear half-access channels shown in the figure and binds to and unbinds from its conserved Glu/Asp-61 binding site on the c-subunit lying within the electrostatic field of the bound succinate anion [30]. These principles are similar to those uncovered recently from pioneering X-ray structural studies on coupled Na^+–succinate cotransporters of the DASS family [83–85]. The change in local electrical potential, $\Delta\Delta\psi$ due to the binding and unbinding events and subsequent ion pair recombination causes electrostatic interaction between the charges on the a- and c-subunits that leads to mechanical rotation, and ultimately to torsional energy storage in the γ-subunit of F_1 to be utilized thereafter for formation of ATP, as detailed in Nath's torsional mechanism of energy transduction and ATP synthesis [30, 34, 37, 49, 52–55, 66]
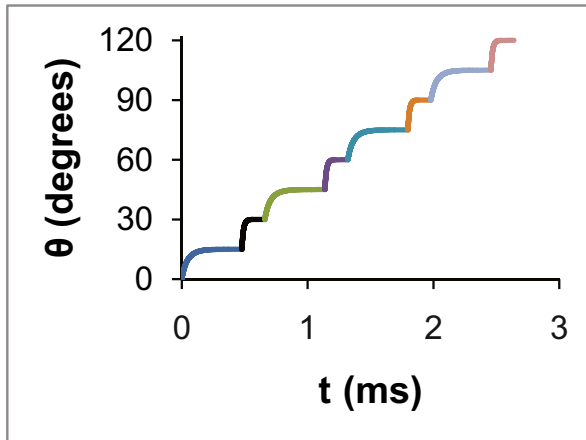
trailing rotor residue and the upper stator residue at any instant of time with respect to the local equilibrium position.

The dynamics of the system can be obtained by simulating in two 15° sub-steps the equation of motion

$$\zeta \frac{d\theta'}{dt} = \tau_{m,d} - \tau_{m,r} \tag{27}$$

with the initial condition

$$\theta' = 0 \text{ at } t = 0 \tag{28}$$

Fig. 10 Dynamics of angular rotation in two discrete 15° elementary substeps for c-rings with 12 c-subunits. The dynamics are quantified by solution of the equations of motion for the $F_O F_1$-ATP synthase enzyme molecule. The values of the parameters used in the simulation are as follows: $\zeta = 2.5 \times 10^{-25}$ kg m^2 s^{-1}; $d = 0.25 \times 10^{-9}$ m; $l_{23} = 1.3 \times 10^{-9}$ m; $r_{12} = 0.65 \times 10^{-9}$ m; $r_{34} = 0.65 \times 10^{-9}$ m; $l_{34} = 0.65 \times 10^{-9}$ m; $\varepsilon_m = 4$. Each 30° step takes approximately 0.66 ms, and one ATP molecule is made per 120° rotation. This leads to a rotational frequency of ~130 Hz, in accord with the experimental value for maximal rate of ATP synthesis of 400 ATP s^{-1} $F_O F_1^{-1}$ by the bacterial ATP synthase [86]

In Eq. (27), $\tau_{m,d}$ is the instantaneous driving electrostatic motor torque, and $\tau_{m,r}$ is the resisting electrostatic motor torque due to the charge geometry (Fig. 9). The solution of the equation of motion yields the angular displacement–time dynamics which is shown in Fig. 10. The parameters used in the simulation are given in the legend to Fig. 10 (see also ref. [30]). A major difference between the previous simulation [30] and this one (Fig. 10) is that at that time, the existence of 15° sub-steps in the rotatory motion of the c-rotor had not been known to occur. Moreover, the intermediate mechanical drive between c-ring rotation and rotation and twist of the γ-subunit of F_1 was not simulated at that time, which is now modeled as rotation θ'' about the axis of the c-subunits arranged in parallel in the helix ring constituting the c-oligomer and twist of the C-terminal c-subunit α-helices of the c-ring [30, 53]. A timescale of ~0.66 ms for a $(15+15)=30°$ step involving bistability is found, leading to a rotational frequency for the enzyme of ~130 Hz (Fig. 10).

The salient details of the simulation, how the parameter values were selected, and other differences from a prior simulation [30] are provided next, in compliance with the second reviewer's suggestion. Since we are dealing with a quantum of energy required to synthesize a molecule of ATP of > 25 kT, random Brownian forces on the order of ~1 kT were neglected in the Langevin equations of motion. The moment of inertia, I, of the c- and γ-subunits was calculated as $\sum_i \left(m_i r_i^2 \right)$ for all atoms of the c- and γ-subunits based on extant X-ray structures [69, 71]. This resulted in an I value of $< 4.5 \times 10^{-37}$ kg m^2 for the subunits. Hence, the inertial terms in the previous simulation [30] could be neglected, given that each term was > 15 orders of magnitude smaller than the other terms in the dynamical equations of motion. We also verified numerically that the inertial terms did not make any perceptible contribution at the microsecond to millisecond timescale of the simulations. This therefore led to a simplified dynamical equation with focus on the electrostatic and mechanical aspects of the energy transduction process.

Fig. 11 Net electrostatic motor torque, $\tau_{m,net}$, and its components $\tau_{m,d}$ and $\tau_{m,r}$ as a function of rotary angle, θ, over one-fourth of the conformational cycle in the F_O portion of ATP synthase
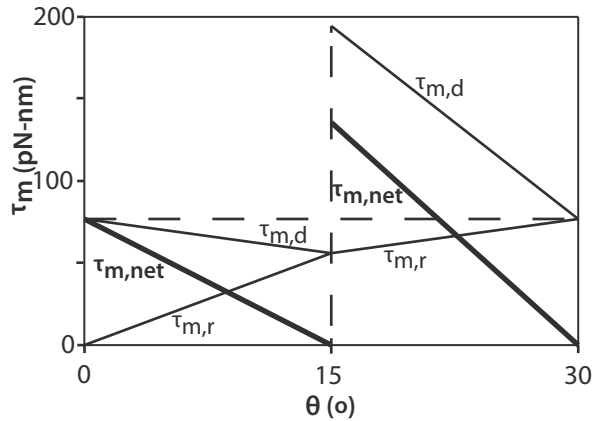
The parameters of the simulation were selected based on available high-resolution structural information on F_O. Given the diameter of the c-ring of 5 nm [68, 69], the distance between two carboxylate binding sites on adjacent c-subunits (l_{23}) could be estimated to measure 1.3 nm. The distances r_{12}, r_{34}, and l_{34} were taken as one-half of the value of l_{23}. We view this choice of distance parameters as an improvement over values in the previous simulation [30]. Not only does this choice obey symmetry principles and is aesthetically elegant, but it also ensures that local equilibrium of the c-rotor–a-stator system is reached at regular angular intervals of $360°/n$, or every 30° for $n = 12$ [28, 30], which is also stable to rotational Brownian fluctuations. The value of the frictional coefficient is in accord with drag studies in the fields of biopolymers and molecular motors [72–74].

The differential equation (Eq. (27)) was solved numerically by the Runge–Kutta fourth-order method. The relationship between θ' and θ was derived trigonometrically for both $\theta = 0–15°$ and $\theta = 15–30°$ sub-steps. Numerical simulation of several test cases revealed that a *linear* electrostatic motor torque vs. θ' or θ was obtained in all cases. With respect to θ', the relationship showed a perfect straight line $\left(R^2 = 1.0\right)$. It is remarkable that a simple, perfectly linear relationship results from such a complex charge geometry (Fig. 9) involving trigonometric functions and polynomial distance formulae [30]. What is the underlying reason for this interesting observation arising from the simulations, which offers tantalizing clues to the molecular mechanism of ATP synthesis? The simulation of the system dynamics (Fig. 10) offers several novel insights into biological energy transduction. The driving electrostatic motor torque, $\tau_{m,d}$, the resisting motor torque, $\tau_{m,r}$, due to the charge geometry, and their difference which gives the net motor torque, $\tau_{m,net}$ (Fig. 11), are determined by electrostatic interactions between the charges on a-stator–c-rotor upon ion pair binding/unbinding. $\tau_{m,net}$ is found to decrease linearly as a function of both θ' and θ over a 15° interval, from 75.8 to 0 pN-nm for the 0–15° sub-step and from 138 to 0 pN-nm for the 15–30° sub-step (Fig. 11). Since the electrostatic forces are time-variant, $\tau_{m,net}$ and its components also vary with time. The underlying reason for a *linear* torque–angle relationship lies in the need to balance the conservative force between the charges by elastic forces. This necessitates the presence of the intermediate drive of the c-subunits in the c-ring of F_O that twist and store torsional energy before transferring their torsional energy to the γ-subunit to enable ATP synthesis [30, 52–54].

Given the new understanding, it is of great importance to model the mechanics of c-subunit deformation in F_O. First, an estimate of the linear spring constant of the c-subunit C-terminal

helix is made from the theory of elasticity. The formula for elastic energy storage, U, is given by

$$U = \frac{\pi R^4 E}{8L(1+\sigma)} \theta''^2 \tag{29}$$

where R and L are the radius and length of the α-helix, respectively, E is the Young's modulus, and σ the Poisson's ratio. From X-ray and cryo-EM data on densely packed c-rings in F_O [68, 69], as also from a statistical analysis of α-helices in protein databases [75], $R = 0.7$ nm. This dimension is also in consonance with the value of $l_{23} = 1.3$ nm employed in the simulations, which should approximately measure $2R$. With $L = 0.7$ nm, $E = 1.8 \times 10^9$ N m^{-2}, and $\sigma = 0.4$, this yields $k'' = 4.8 \times 10^{-20}$ kg m^2 s^{-2}. Hence k''_{eq} for the $(n-2) = (12-2) = 10$ twisting c-subunits arranged in parallel in the c-ring works out to be 4.8×10^{-19} kg m^2 s^{-2}. For the 0–15° sub-step with an initial $\tau_{m,net} = 75.8$ pN-nm (Fig. 11), $\theta'' = 75.8 \times 10^{-21}/4.8 \times 10^{-19} = 0.1566$ radians, implying a torsional energy storage $\frac{1}{2} k''_{eq} \theta''^2$ in the c-ring helices of 3.5 kJ mol^{-1}. Similarly for the 15–30° sub-step with an initial $\tau_{m,net} = 138$ pN-nm (Fig. 11), $\theta'' = 138 \times 10^{-21}/4.8 \times 10^{-19} = 0.285$ radians, leading to energy storage $\frac{1}{2} k''_{eq} \theta''^2$ in the c-ring helices of 11.8 kJ mol^{-1} as twist energy. Hence, the total energy stored as twist in the c-ring for a 30° rotation equals 15.3 kJ mol^{-1}. For 120° rotation corresponding to synthesis of one ATP molecule, this provides a stored energy of $15.3 \times 4 = 61.2$ kJ mol^{-1}, which adequately meets the energy requirements for synthesis. The maximum angle of rotation θ'' about the axis of a single c-subunit, if it were alone, would be $2.85 \times 57.3 = 160°$, in agreement with the value determined experimentally using NMR spectroscopy by comparison of the solution structure of an unprotonated c-subunit with the structure of the protonated c-subunit [76].

Furthermore, from the standpoint of $\tau_{m,net}$, taking the area under the curve of the $\tau_{m,net}$–θ relationship obtained from the simulation (Fig. 11), the total torsional energy storage per 30° rotation works out to be $\left(9.9 \times 10^{-21} + 18.1 \times 10^{-21}\right) = 28$ pN-nm, or $(5.9 + 10.8) = 16.7$ kJ mol^{-1}, which corresponds to ~ 67 kJ mol^{-1} for one catalytic cycle of 120° (Fig. 10). Hence, the above analysis shows that the physical, chemical, and energetic requirements of ATP synthesis are met adequately, that constraints arising from experimental data are satisfied, and that excellent agreement is obtained with all available experimental information by the results of the simulation (Figs. 10 and 11).

The present simulation also explains why the previous simulation [30] worked satisfactorily, although it did not incorporate the "*wheels-within-wheels*" detailed molecular mechanism of twisting of the c-subunits in the c-ring during ATP synthesis, first proposed back in 2002 ([30, 53]; see esp. pp. 90–93 and Fig. 12 in [30]) and modeled in this work. Neglecting inertia, the equation of motion of the previous simulation [30] can be recast as

$$\zeta \frac{d\theta'}{dt} = \tau_{m,d} - k\theta \tag{30}$$

In Eq. (30), as in the prior simulation [30], k is the torsional spring constant of the γ-subunit in F_1. However, there is no *direct* interaction between the c-rotor in F_O and the γ-subunit in F_1 — they each interact directly only with the common intermediary of the c-subunit α-helices of the c-rotor in F_O. But since we have a resisting motor torque, $\tau_{m,r}$, that is linear with angular displacement, as shown in Fig. 11, the $k\theta$ in Eq. (30) inadvertently modeled, or rather mimicked, $\tau_{m,r}$, as readily seen by comparing Eq. (27) with Eq. (30). Hence, phenomenologically, the right results were obtained earlier, although the

actual physical situation was not fully realized, and the detailed molecular mechanism within F_O was not incorporated in the previous simulation [30]. The present simulation takes us a step deeper in our understanding of the process of energy storage and transduction in ATP synthase, and in molecular motors in general.

The above discussion has clarified the important point that if θ'' was identical to θ (or θ'), then as θ increases from 0 to 15 degrees during c-ring rotation (Fig. 10), $k\theta$ in the linear springs of the c-subunit α-helices can only increase, implying that there will only be energy storage as twist, but never any energy release. Hence, for efficient *release* of stored energy, there is the absolute requirement of an intermediate drive between the γ-subunit and the electrostatic torque at the a–c interface, e.g., as twist of c-helices by rotation, θ'', about their own axis. Thus, we are led to the conclusion that in response to the initial impulse of the net electrostatic torque, $\tau_{m,net}$, θ'' also increases very fast and the c-subunit springs of the c-ring twist until their $k''_{eq}\theta''$ balances $\tau_{m,net}$. However, $\tau_{m,net}$ is a continually *decreasing* function of θ as θ progresses over a 15° angular interval.

Thus, once $k''_{eq}\theta''$ balances $\tau_{m,net}$ close to $\theta \sim 0°$, since $\tau_{m,net}$ itself is a decreasing torque due to the charge geometry (i.e., due to non-mechanical reasons), the θ'' will start decreasing, i.e., untwisting occurs, and the $k''_{eq}\theta''$ will always *dynamically* balance the $\tau_{m,net}$ over the entire range of θ during the release process. Since $\tau_{m,net}$ does not decrease to 0 instantaneously, $k''_{eq}\theta''$ also does not disappear instantaneously but follows the torque. Furthermore, this untwisting energy of the c-subunit helices is off-loaded to the γ-subunit. The energy stored in γ as torsional energy works out to be ~ 60 kJ mol^{-1} over a 120° interval in the simulation (Figs. 10 and 11), which is thermodynamically competent to synthesize one mole of ATP [47, 50, 54, 62].

In summary, the twisting of the c-helices is very fast in response to the motor torque but the release of torsional energy is slow and is distributed over most of the 15° rotation cycle in F_O during ATP synthesis. Thus, the applied torsional spring force balances the inertial conservative electrostatic force during the energy release process. This leads to a most efficient transduction of energy in ATP synthesis by ATP synthase.

3.9 A meeting ground for physics, chemistry, and biology

This work has presented the first analysis of ion translocation and energy transduction in membrane transporters from a Gibbs energy landscape perspective. The dynamic regulation of the transport of ions and other polar metabolites through a lipid barrier represents a vital biological attribute of all cells. The complex membrane system requires a study of its structure, architecture, connectivity, interaction, and function that is reflective of life processes, a central topic of biologists. Yet analysis of the biological system requires physics, e.g., by electrostatic theories that quantify Gibbs energy landscapes, phase-transition in frustrated systems, and elucidation of system dynamics by Langevin, Fokker–Planck, or similar equations of motion. These properly constitute the subject matter of physics. However, the translocation of ions through membrane transporters and the ion-protein interactions that are crucial to biological energy transduction traditionally belong to the domain of physical chemistry, as do the thermodynamics of these processes. In fact, even the concept of Gibbs energy itself may be regarded as a mainstay of chemists. In this work, concepts from the above fields have been integrated from an energy landscape perspective. It is shown by physical analysis that membrane-bound enzymes, transporters, and molecular machines such as the F_OF_1-ATP synthase can be treated as a microcosm in which many fundamental concepts from physics, chemistry, and biology are reflected.

4 Conclusions

A large number of conclusions on ion translocation and dynamics of membrane transporters were arrived at in this study based on a novel analytical framework of Gibbs energy landscapes.

1.   Current models of ion translocation through membrane transporters do not take into account the self-energy of the relevant charges, which is a serious lacuna of these models.

2.   The macroscopic Kirkwood–Tanford–Warshel (KTW) electrostatic theory, originally developed for spherical membranous phases, has been extended and shown to be applicable to planar membranes also. The KTW theory properly takes into account the self-energies of the ions, has the ability to accurately evaluate the electrostatic Gibbs energy of a system of charges, and possesses great conceptual power. It provides a simple model based on continuum electrostatic considerations that offers valuable insights into complex bioenergetic and membrane transport processes, without performing detailed or exact calculations or all-atom molecular dynamics simulations. The theory can be readily extended, and the reliability of calculations further enhanced, by use of semi-macroscopic or microscopic electrostatic theories as further experience is gained by applying them to many biological systems and processes.

3.   The calculated Gibbs energy landscape for a single species of translocated ion versus translocation of a proton–anion charge pair through a membrane transporter show qualitatively very different characteristics. An important feature is that the Gibbs energy asymptotes to a large positive (destabilizing) value for translocation of a single ion species, owing to the high self-energy of the process. Thus, the energy barrier cannot be lowered to 0 for a charge configuration involving only a single type of ion.

4.   On the other hand, for a charge pair, the adverse $\Delta G_{desolvation}$ is almost completely compensated by the sum of the electrostatic Gibbs energy of the charge–charge interactions and the solvation energy of the ion pair. In essence, between two stable low Gibbs energy states, corresponding to a long-range ion pair and chemical bond formation of an uncharged substrate HA, a maxima in $\Delta G_{KTW}(R)$ is found at an intermediate value of the interionic distance, R, corresponding to an $[\text{E–H}^+\text{A}^-]^*$ "*high-energy charge-pair intermediate*" on the enzyme. The difference in Gibbs energy between the maxima and the low Gibbs energy state is transduced and stored in local domains of the macromolecule and can be used thereafter for the performance of useful external work.

5.   The electrostatic Gibbs energy involving an ion pair can therefore be regarded as another illustration of a *frustrated* system involving *bistability* that shows a *maxima* at intermediate values of the order parameter. Hence, the physics of first-order phase transitions can be applied to gain further valuable insights into the process.

6.   The theoretically calculated Gibbs energy landscape for ion pairs has been compared using experimental data from NMR spectroscopy for a number of globular proteins, and good agreement between theory and experiment has been shown.

7.   Proton-only and all single-ion theories of ATP synthesis, such as the chemiosmotic theory, are inadequate to understand energy transduction and storage in bioenergetic processes.

8.   By including the key roles of both proton and anion that translocate in a sequential, coupled way to form an enzyme-bound $H^+ - A^-$ charge pair in half-access channels of membrane transporters such as the $F_O F_1$-ATP synthase, Nath's torsional mechanism of energy transduction and ATP synthesis and Nath's two-ion theory of energy coupling offer novel insights and lead to a superior understanding of energy transduction at the molecular level.

9. The net ΔG_{KTW} tends to a value of ~ 0 at a finite separation distance of H^+ and A^- ($\sim 10\text{Å}$) due to complete Gibbs energy compensation arising from ion-ion coupling by local fields. The profiles of the local electrical field and the local electrical potential have been shown to be amenable to analytical derivation by direct solution of Poisson's equation. The *localized coupling within membrane transporters* has been concluded to be caused physically by interaction between the electrical layers around the positive and negative space-charge regions. The necessary condition for coupling has been shown to be $\lambda \sim R < \lambda_D$. Thus, an analysis of system scale sizes has been shown to shed light on molecular mechanism in ATP synthase. These fundamental physical concepts should be applicable to other mesoscopic systems also.

10. The timescale at which the mechanochemical enzyme/transporter system moves between the two stable states of the frustrated system has been shown to be estimated by simulation of the dynamics of torque generation. This works out to measure approximately two-thirds of a millisecond for ATP synthesis by the $F_O F_1$-ATP synthase.

11. Quantification of the dynamics of the enzyme/transporter system has been shown to offer a wealth of novel mechanistic insights and help infer conditions for efficient transduction of energy during ATP synthesis by the $F_O F_1$-ATP synthase. These include the necessity of an intermediate mechanical drive of the c-subunits in the c-ring of F_O that twists, stores elastic energy, and subsequently untwists and transfers the stored energy to the central γ-subunit as torsional energy that is used thereafter for ATP synthesis in F_1. The energy storage in the c-subunits due to ion binding/unbinding and ion-protein interactions in F_O is almost instantaneous and thus "discrete," while the energy release from the c-subunits to the γ-subunit is slow, "continuous," and distributed throughout the $\sim 15°$ rotation cycle of the c-rotor during the process of ATP synthesis. These features of balanced energy release have been shown to lead to the most efficient energy transfer in ATP synthase.

12. The unifying analytical framework developed here for Gibbs energy landscapes in membrane-bound enzymes, membrane transporters, and biological molecular machines such as the $F_O F_1$-ATP synthase have been shown to provide a meeting ground for physics, chemistry, and biology. They can also serve as a reliable guide for the design and fabrication of efficient mechanochemical devices in nanoscience and nanotechnology applications [34, 53].

13. The unified framework of Gibbs energy landscapes has been shown to provide the essential features of biological energy coupling, transduction, and ATP synthesis by membrane transporters that should not be overlooked by further work in this important field of contemporary interdisciplinary research. In summary, the revolutionary impact of energy landscapes to fundamental biological processes stands accentuated.

Declarations

Competing interests The author declares no competing interests.

References

1. Gould, S.J.: Punctuated Equilibrium. Harvard University Press, Cambridge, MA, USA (2007)
2. Moran, N.A.: Accelerated evolution. Proc. Natl. Acad. Sci. USA **93**, 2873–2878 (1996)
3. Romero, P.A., Arnold, F.H.: Exploring protein fitness landscapes by directed evolution. Nature Rev. Mol. Cell Biol. **10**, 866–876 (2009)
4. Zhang, Q.C., et al.: Acceleration of emergence of bacterial antibiotic resistance in connected microenvironments. Science **333**, 1764–1767 (2011)
5. Austin, R.H., Beeson, K.W., Eisenstein, L., Frauenfelder, H., Gunsalus, I.C.: Dynamics of ligand binding to myoglobin. Biochemistry **14**, 5355–5373 (1975)
6. Ansari, A., Berendzen, J., Bowne, S.F., Frauenfelder, H., Iben, I.E.T., Sauke, T.B., Shyamsunder, E., Young, R.D.: Protein states and proteinquakes. Proc. Natl. Acad. Sci. USA **82**, 5000–5004 (1985)
7. Janke, W.: Rugged Free Energy Landscapes: Common Computational Approaches to Spin Glasses, Structured Glasses and Biological Macromolecules. Springer, Berlin (2010)
8. Bryngelson, J.D., Wolynes, P.G.: Spin-glasses and the statistical-mechanics of protein folding. Proc. Natl. Acad. Sci. USA **84**, 7524–7528 (1987)
9. Shakhnovich, E.: Protein folding thermodynamics and dynamics: where physics, chemistry, and biology meet. Chem. Rev. **106**, 1559–1588 (2006)
10. Frauenfelder, H.: Energy landscape and dynamics of biomolecules. J. Biol. Phys. **31**, 413–416 (2005)
11. Holmes-Cerfon, M., Gortler, S.J., Brenner, M.P.: A geometrical approach to computing free-energy landscapes from short-ranged potentials. Proc. Natl. Acad. Sci. USA **109**, E5–E14 (2012)
12. Hénin, J., Fiorin, G., Chipot, C., Klein, M.L.: Exploring multidimensional free energy landscapes using time-dependent biases on collective variables. J. Chem. Theory Comput. **6**, 35–47 (2010)
13. Radak, B.K., Phillips, J.C., Jiang, W., Jo, S., Kalé, L., Schulten, K., Roux, B.: Free energy landscapes of membrane transport proteins. Technical Report ANL/ALCF/ESP–17/11 for the Argonne Leadership Computing Facility Theta Early Science Program (Williams, T.J., Balakrishnan, R., Eds.), Argonne National Laboratory (2017)
14. Selvam, B., Mittal, S., Shukla, D.: Free energy landscape of the complete transport cycle in a key bacterial transporter. ACS Cent. Sci. **4**, 1146–1154 (2018)
15. Lu, H., Marti, J.: Cellular absorption of small molecules: free energy landscapes of melatonin binding at phospholipid membranes. Sci. Rep. **10**, 9235 (2020)
16. Crossley, J.A. et al.: Energy landscape steering in SecYEG mediates dynamic coupling in ATP driven protein translocation. bioRxiv preprint. https://doi.org/10.1101/793943 (2020)
17. Bacchin, P.: Membranes: a variety of energy landscapes for many transfer opportunities. Membranes **8**, 10 (2018)
18. Kornberg, R.D., McNamee, M.G., McConnell, H.M.: Measurement of transmembrane potentials in phospholipid vesicles. Proc. Natl. Acad. Sci. USA **69**, 1508–1513 (1972)
19. Burykin, A., Warshel, A.: What really prevents proton transport through aquaporin? Charge self-energy versus proton wire proposals. Biophys. J. **85**, 3696–3706 (2003)
20. Shirai, O., Yoshida, Y., Matsui, M., Maeda, K., Kihara, S.: Voltammetric study on the transport of ions of various hydrophobicity types through bilayer lipid membranes composed of various lipids. Bull. Chem. Soc. Japan **69**, 3151–3162 (1996)
21. Laforge, F.O., Sun, S., Mirkin, M.V.: Shuttling mechanism of ion transfer at the interface between two immiscible liquids. J. Am. Chem. Soc. **128**, 15019–15025 (2006)
22. Soumpasis, D.M., Jovin, T.M.: Computation of Biomolecular Structures: Achievements. Problems and Perspectives. Springer, Berlin (1993)
23. Zhang, J., Kamenev, A., Shklovskii, B.I.: Conductance of ion channels and nanopores with charged walls: a toy model. Phys. Rev. Lett. **95**, 1488101 (2005)
24. Mulkidjanian, A.Y.: Proton in the well and through the desolvation barrier. Biochim. Biophys. Acta **1757**, 415–427 (2006)
25. Morelli, A.M., Ravera, S. Calzia, D., Panfoli, I.: An update of the chemiosmotic theory as suggested by possible proton currents inside the coupling membrane. Open Biol. **9**, 180221 (2019)
26. Williams, R.J.P.: The problem of proton transfer in membranes. J. Theor. Biol. **219**, 389–396 (2002)
27. Mitchell, P.: Chemiosmotic coupling in oxidative and photosynthetic phosphorylation. Biol. Rev. **41**, 445–502 (1966)
28. Rohatgi, H., Saha, A., Nath, S.: Mechanism of ATP synthesis by protonmotive force. Curr. Sci. **75**, 716–718 (1998)

29. Lebon, G., Jou, D., Casas-Vázquez, J.: Understanding Non-equilibrium Thermodynamics: Foundations, Applications, Frontiers. Springer, Berlin (2008)
30. Nath, S.: The molecular mechanism of ATP synthesis by F_1F_0-ATP synthase: a scrutiny of the major possibilities. Adv. Biochem. Eng. Biotechnol. **74**, 65–98 (2002)
31. Jain, S., Murugavel, R., Hansen, L.D.: ATP synthase and the torsional mechanism: resolving a 50-year-old mystery. Curr. Sci. **87**, 16–19 (2004)
32. Villadsen, J., Nielsen, J., Lidén, G.: Bioreaction Engineering Principles, 3rd edn. Springer, New York (2011). (Chapter 4)
33. Wray, V.: Commentary on "Oxidative phosphorylation revisited." Biotechnol. Bioeng. **112**, 1984–1985 (2015)
34. Nath, S.: Molecular mechanisms of energy transduction in cells: engineering applications and biological implications. Adv. Biochem. Eng. Biotechnol. **85**, 125–180 (2003)
35. Bal, W., Kurowska, E., Maret, W.: The final frontier of pH and the undiscovered country beyond. PLoS ONE **7**, e45832 (2012).
36. Żurawik, T.M. et al.: Revisiting mitochondrial pH with an improved algorithm for calibration of the ratiometric 5(6)-carboxy-SNARF-1 probe reveals anticooperative reaction with H^+ ions and warrants further studies of organellar pH. PLoS ONE **11**, e0161353 (2016)
37. Nath, S.: The torsional mechanism of energy transduction and ATP synthesis as a breakthrough in our understanding of the mechanistic, kinetic and thermodynamic details. Thermochim. Acta **422**, 5–17 (2004)
38. Warshel, A., Russell, S.T.: Calculations of electrostatic interactions in proteins and in solutions. Q. Rev. Biophys. **17**, 283–422 (1984)
39. von Kitzing, E., Soumpasis, D.M.: Electrostatics of a simple membrane model using Green's functions formalism. Biophys. J. **71**, 795–810 (1996)
40. Zhang, J., Kamenev, A., Shklovskii, B.I.: Ion exchange phase transitions in water-filled channels with charged walls. Phys. Rev. E **73**, 051205 (2006)
41. Bonthuis, D.J., Zhang, J., Hornblower, B., Mathe, J., Shklovskii, B.I., Meller, A.: Self-energy-limited ion transport in subnanometer channels, Phys. Rev. Lett. **97**, 128104 (1996)
42. Chen, H., Ilan, B., Wu, Y., Zhu, F., Schulten, K., Voth, G.A.: Charge delocalization in proton channels: the aquaporin channels and proton blockage. Biophys. J. **92**, 46–60 (2007)
43. Ivanischev, V.V.: Problems of the mathematical description of the chemiosmotic theory. News Tula State Univ. Natl. Sci. **3**, 129–135 (2018)
44. Levy, W.B., Calvert, V.G.: Communication consumes 35 times more energy than computation in the human cortex, but both costs are needed to predict synapse number. Proc. Natl. Acad. Sci. USA **118**, e2008173118 (2021)
45. Karapetyan, L., Mikoyan, G., Vassilian, A., Valle, A., Bolivar, J., Trchounian, A., Trchounian, K.: *Escherichia coli* Dcu C_4-dicarboxylate transporters dependent proton and potassium fluxes and F_OF_1-ATPase activity during glucose fermentation at pH 7.5. Bioelectrochemistry **141**, 107867 (2021)
46. Bose, H.S., Marshall, B., Debnath, D.K., Perry E.W., Whittal, R.M.: Electron transport chain complex II regulates steroid metabolism. iScience **23**, 101295 (2020)
47. Nath, S.: Entropy production and its application to the coupled nonequilibrium processes of ATP synthesis. Entropy **21**, 746 (2019)
48. Nath, S.: Two-ion theory of energy coupling in ATP synthesis rectifies a fundamental flaw in the governing equations of the chemiosmotic theory. Biophys. Chem. **230**, 45–52 (2017)
49. Nath, S.: Beyond the chemiosmotic theory: analysis of key fundamental aspects of energy coupling in oxidative phosphorylation in the light of a torsional mechanism of energy transduction and ATP synthesis. J. Bioenerg. Biomembr. **42**, 301–309 (2010)
50. Nath, S.: Analysis of molecular mechanisms of ATP synthesis from the standpoint of the principle of electrical neutrality. Biophys. Chem. **224**, 49–58 (2017)
51. Nath, S.: Optimality principle for the coupled chemical reactions of ATP synthesis and its molecular interpretation. Chem. Phys. Lett. **699**, 212–217 (2018)
52. Nath, S., Rohatgi, H., Saha, A.: The torsional mechanism of energy transfer in ATP synthase. Curr. Sci. **77**, 167–169 (1999)
53. Nath, S., Jain, S.: The detailed molecular mechanism of ATP synthesis in the F_0 portion of ATP synthase reveals a non-chemiosmotic mode of energy coupling. Thermochim. Acta **394**, 89–98 (2002)
54. Nath, S.: The new unified theory of ATP synthesis/hydrolysis and muscle contraction, its manifold fundamental consequences and mechanistic implications and its applications in health and disease. Int. J. Mol. Sci. **9**, 1784–1840 (2008)
55. Nath, S.S., Nath, S.: Energy transfer from adenosine triphosphate: Quantitative analysis and mechanistic insights. J. Phys. Chem. B **113**, 1533–1537 (2009)

56. Kirkwood, J.G.: Theory of solutions of molecules containing widely separated charges with special application to zwitterions. J. Chem. Phys. **2**, 351–361 (1934)
57. Tanford, C., Kirkwood, J.G.: Theory of protein titration curves. I. General equations for impenetrable spheres. J. Am. Chem. Soc. **79**, 5333–5339 (1957)
58. Born, M.: Volumen und Hydratationswärme der Ionen. Z. Phys. **1**, 45–48 (1920)
59. Onsager, L.: Electric moments of molecules in liquids. J. Am. Chem. Soc. **58**, 1486–1493 (1936)
60. Shockley, W.: The theory of *p-n* junctions in semiconductors and *p-n* junction transistors. Bell Syst. Tech. J. **28**, 435–489 (1949)
61. Warshel, A., Schlosser, D.W.: Electrostatic control of the efficiency of light-induced electron transfer across membranes. Proc. Natl. Acad. Sci. USA **78**, 5564–5568 (1981)
62. Nath, S.: The thermodynamic efficiency of ATP synthesis in oxidative phosphorylation. Biophys. Chem. **219**, 69–74 (2016)
63. Nath, S.: Modern theory of energy coupling and ATP synthesis. Violation of Gauss's law by the chemiosmotic theory and validation of the two-ion theory. Biophys. Chem. **255**, 106271 (2019)
64. Mitchell, P.: Bioenergetic aspects of unity in biochemistry: evolution of the concept of ligand conduction in chemical, osmotic and chemiosmotic reaction mechanisms. In: Semenza, G. (ed.) Of Oxygen, Fuels and Living Matter, Part 1, pp. 30–56. John Wiley, New York (1981)
65. Williams, R.J.P.: Some unrealistic assumptions in the theory of chemi-osmosis and their consequences. FEBS Lett. **102**, 126–132 (1979)
66. Nath, S.: Consolidation of Nath's torsional mechanism of ATP synthesis and two-ion theory of energy coupling in oxidative phosphorylation and photophosphorylation. Biophys. Chem. **257**, 106279 (2020)
67. Nath, S.: Coupling mechanisms in ATP synthesis: rejoinder to "Response to molecular-level understanding of biological energy coupling and transduction". Biophys. Chem. **272**, 106579 (2021)
68. Kühlbrandt, W., Davies, K.M.: Rotary ATPases: a new twist to an ancient machine. Trends Biochem. Sci. **41**, 106–115 (2016)
69. Schulz, S., Iglesias-Cans, M., Krah, A., Yildiz, Ö., Leone, V., Matthies, D., Cooke, G.M., Faraldo-Gómez, J.D., Meier, T.: A new type of Na⁺-driven ATP synthase with a two-carboxylate ion-coupling motif. PLoS Biol. **11**, e1001596 (2013). https://doi.org/10.1371/journal.pbio.1001596
70. Pinke, G., Zhou, L., Sazanov, L.A.: Cryo-EM structure of the entire mammalian F-type ATP synthase. Nature Str. Mol. Biol. **27**, 1077–1085 (2020)
71. Abrahams, J.P., Leslie, A.G.W., Lutter, R., Walker, J.E.: Structure at 2.8 Å resolution of F₁–ATPase from bovine heart mitochondria. Nature **370**, 621–628 (1994)
72. Nath, S., Bowers, J.S., Prud'homme, R.K.: Orientation and relaxation of nonlinear elastic dumbbells in electric fields: modeling transient electric birefringence. J. Chem. Phys. **89**, 5943–5949 (1988)
73. Nath, S., Siddiqui, R.S.: Transient electric birefringence of flexible polymers: orientation and relaxation dynamics. J. Chem. Phys. **103**, 3212–3219 (1995)
74. Mandadapu, K.K., Nirody, J.A., Berry, R.M., Oster, G.: Mechanics of torque generation in the bacterial flagellar motor. Proc. Natl. Acad. Sci. USA **112**, E4381–E4389 (2015)
75. Kumar, S., Bansal, M.: Geometrical and sequence characteristics of α-helices in globular proteins. Biophys. J. **75**, 1935–1944 (1998)
76. Rastogi, V.K., Girvin, M.E.: Structural changes linked to proton translocation by subunit c of the ATP synthase. Nature **402**, 263–268 (1999)
77. Kumar, S., Nussinov, R.: Relationship between ion pair geometries and electrostatic strengths in proteins. Biophys. J. **83**, 1595–1612 (2002)
78. Bosshard, H.R., Zürrer, M.: The conformation of cytochrome in solution. Localization of a conformational difference between ferri- and ferrocytochrome c on the surface of the molecule. J. Biol. Chem. **255**, 6694–6699 (1980)
79. Kilmartin, J.V., Fogg, J.H., Perutz, M.F.: Role of C-terminal histidine in the alkaline Bohr effect of human haemoglobin. Biochemistry **19**, 3189–3193 (1980)
80. Parsons, S.M., Raftery, M.A.: Ionization behavior of the catalytic carboxyls of lysozyme. Effects of ionic strength. Biochemistry **11**, 1623–1629 (1972)
81. Rees, D.C.: Experimental evaluation of the effective dielectric constant in proteins. J. Mol. Biol. **141**, 323–326 (1980)
82. Nath, S., Villadsen, J.: Oxidative phosphorylation revisited. Biotechnol. Bioeng. **112**, 429–437 (2015)
83. Mancusso, R., Gregorio, G.G., Liu, Q., Wang, D-N.: Structure and mechanism of a bacterial sodium-dependent dicarboxylate transporter. Nature **491**, 622–626 (2012)
84. Sauer, D.B., Wang, B., Sudar, J.C., Song, J., Marden, J., Rice, W.J., Wang, DN.: The ups and downs of elevator-type di/tricarboxylate membrane transporters. FEBS J. 1–9 (2021). https://doi.org/10.1111/febs.16158

85. Sauer, D.B., Trebesch, N., Marden, J.J., Cocco, N., Song, J., Koide, A., Koide, S. Tajkhorshid, E., Wang, D-N.: Structural basis for the reaction cycle of DASS dicarboxylate transporters. eLife **9**, e61350 (2020). https://doi.org/10.7554/eLife.61350

86. Etzold, C., Deckers-Hebestreit, G., Altendorf, K.: Turnover number of *Escherichia coli* F_0F_1 ATP synthase for ATP synthesis in membrane vesicles. Eur. J. Biochem. **243**, 336–343 (1997)

Publisher's Note Springer Nature remains neutral with regard to jurisdictional claims in published maps and institutional affiliations.

Authors and Affiliations

Sunil Nath[1]

✉ Sunil Nath
  sunath@iitd.ac.in; sunil_nath_iit@yahoo.com

[1] Department of Biochemical Engineering and Biotechnology, Indian Institute of Technology Delhi, Hauz Khas, New Delhi 110016, India